Segregating the Frontal Cortex with Deep Brain Stimulation

Barbara Hollunder[1,2,3], Jill L. Ostrem[4], Ilkem Aysu Sahin[1,2], Nanditha Rajamani[1], Simón Oxenford[1], Konstantin Butenko[5], Mircea Polosan[6,7,8], Harith Akram[9,10], Matteo Vissani[11,12,13], Chencheng Zhang[14], Bomin Sun[14], Martin M. Reich[15], Jens Volkmann[15], Carsten Finke[1,2,3], Andrea A. Kühn[1,2,3,16], Hagai Bergman[17,18,19], Mahlon R. DeLong[20], Alberto Mazzoni[11,12], Luigi M. Romito[21], Ludvic Zrinzo[9,10], Eileen M. Joyce[9,10], Stephan Chabardes[6,7,22], Philip A. Starr[23], Ningfei Li[1,*,+], Andreas Horn[1,2,5,13,*,+]

** These authors contributed equally to this work.*

[+] *Corresponding authors.*

Affiliations

1. Department of Neurology, Charité – Universitätsmedizin Berlin, Berlin, Germany
2. Einstein Center for Neurosciences Berlin, Charité – Universitätsmedizin Berlin, Berlin, Germany
3. Berlin School of Mind and Brain, Humboldt-Universität zu Berlin, Berlin, Germany
4. Movement Disorders and Neuromodulation Centre, Department of Neurology, University of California San Francisco, San Francisco, CA, USA
5. Center for Brain Circuit Therapeutics, Department of Neurology, Brigham & Women's Hospital, Harvard Medical School, Boston, MA, USA
6. Université Grenoble Alpes, Grenoble, France
7. Inserm, U1216, Grenoble Institut des Neurosciences, Grenoble, France
8. Psychiatry Department, Centre Hospitalier Universitaire Grenoble Alpes, Grenoble, France
9. Department of Clinical and Movement Neurosciences, University College London Queen Square Institute of Neurology, London, UK
10. National Hospital for Neurology and Neurosurgery, University College London Queen Square Institute of Neurology, London, UK
11. The BioRobotics Institute, Scuola Superiore Sant'Anna, Pisa, Italy
12. Department of Excellence in Robotics and AI, Scuola Superiore Sant'Anna, Pisa, Italy
13. Department of Neurosurgery, Massachusetts General Hospital, Harvard Medical School, Boston, MA, USA
14. Department of Neurosurgery, Rujin Hospital, Shanghai Jiao Tong University School of Medicine, Shanghai, China
15. Department of Neurology, University Hospital Würzburg, Würzburg, Germany
16. NeuroCure Cluster of Excellence, Charité – Universitätsmedizin Berlin, Berlin, Germany
17. The Edmond and Lily Safra Center for Brain Sciences, The Hebrew University, Jerusalem, Israel
18. Department of Medical Neurobiology, Institute of Medical Research Israel-Canada, The Hebrew University, Hassadah Medical School, Jerusalem, Israel
19. Department of Neurosurgery, Hadassah Medical Center, Jerusalem, Israel
20. Department of Neurology, Emory University School of Medicine, Atlanta, GA, USA
21. Parkinson and Movement Disorders Unit, Fondazione IRCCS Istituto Neurologico Carlo Besta, Milan, Italy
22. Neurosurgery department, Centre Hospitalier Universitaire Grenoble Alpes, Grenoble, France
23. Department of Neurological Surgery, University of California San Francisco, San Francisco, CA, USA

Corresponding Authors

Ningfei Li, Movement Disorders and Neuromodulation Unit, Department of Neurology, Charité – Universitätsmedizin Berlin (CCM), Charitéplatz 1, 10117 Berlin, Germany. E-mail: ningfei.li@charite.de

Andreas Horn, Center for Brain Circuit Therapeutics, Department of Neurology, Brigham & Women's Hospital, Harvard Medical School, 75 Francis Street, 02445 Boston, MA, USA. E-mail: ahorn1@bwh.harvard.edu

Keywords

Dystonia, Parkinson's disease (PD), Obsessive-Compulsive Disorder (OCD), Tourette's syndrome (TS), Deep Brain Stimulation (DBS), Subthalamic Nucleus (STN), Connectome, Structural Connectivity

Word counts

Number of words in the abstract*:* 150 / 150

Number of words in the main text: 4,489 / 4,500

Number of display items: 8 / 8

Abstract

The frontal cortex is involved in motor, cognitive, and affective brain functions. In humans, however, neuroanatomy-function mappings are predominantly derived from correlative neuroimaging studies. Hence, exactly which frontal domains *causally* mediate which function remains largely elusive. Herein, we leverage a strategy that allows for causal inference using invasive neuromodulation. Studying 394 subthalamic deep brain stimulation electrodes in patients suffering from one of four brain disorders, we segregated the frontal cortex into cortical projection sites of modulated circuits by their involvement in specific functions. Modulating projections from sensory and motor cortices in dystonia, from primary motor cortex in Tourette's syndrome, from supplementary motor cortex in Parkinson's disease, and from ventromedial prefrontal, anterior cingulate, dorsolateral prefrontal and orbitofrontal cortices in obsessive-compulsive disorder linked to respective symptom improvements. Our findings showcase the combination of deep brain stimulation and brain connectomics as a tool for causal inference on structure-function mappings within the human brain.

Abbreviations

ANTs	Advanced Normalization Tools
BFMDRS	Burke-Fahn-Marsden Dystonia Rating Scale
CIT168 atlas	California Institute of Technology reinforcement learning atlas
CT	computed tomography
DBS	deep brain stimulation
DISTAL	DBS intrinsic template atlas
dMRI	diffusion-weighted magnetic resonance imaging
DYT	dystonia
E-field	electric field magnitude
FEM	finite element method
fMRI	functional magnetic resonance imaging
GPe	external pallidum (globus pallidus, external segment)
GPi	internal pallidum (globus pallidus, internal segment)
HCP	Human Connectome Project
JHU atlas	Johns Hopkins University atlas
MGH	Massachusetts General Hospital
MNI space	ICBM 2009b Non-linear Asymmetric template space
M1	primary motor cortex
MRI	magnetic resonance imaging
OCD	obsessive-compulsive disorder
PD	Parkinson's disease
PaCER algorithm	Precise and Convenient Electrode Reconstruction for Deep Brain Stimulation algorithm
SMA	supplementary motor area
SPM12 software	Statistical Parametric Mapping software
STN	subthalamic nucleus
SyN approach	Symmetric Normalization approach
TRAC/CORE algorithm	trajectory search/contact reconstructions algorithm
TS	Tourette's syndrome
UPDRS-III	Unified Parkinson's Disease Rating Scale – Part III
Y-BOCS	Yale-Brown Obsessive-Compulsive Scale
YGTSS	Yale Global Tic Severity Scale

Interactions between the frontal cortex and basal ganglia are implicated in motor, cognitive, and affective functions – and their disruption gives rise to multifarious brain disorders [1,2]. These functional domains are anatomically realized in the form of fronto-subcortical neurocircuits that cross-communicate [3,4], but retain a certain amount of segregation at each node, i.e., on cortical, striatal, pallidal/nigral and thalamic levels [3–7]. While the striatum is often described as the main input structure of the basal ganglia, the subthalamic nucleus (STN) has recently been acknowledged as a second direct input nucleus [8]. The STN – with a volume of only ~240 mm^3 [9] – is much smaller than the striatum, but nonetheless receives efference copies of projections from the entire frontal cortex [3], rendering it an ideal access node to modulate large-scale brain networks using small electrodes. Indeed, the nucleus has been successfully targeted by deep brain stimulation (DBS) to treat diseases as different as Parkinson's disease (PD) [10], dystonia (DYT) [11,12], obsessive-compulsive disorder (OCD) [13,14], and Tourette's syndrome (TS) [15,16].

In animal models, the functional involvement of distinct fronto-subcortical fiber bundles has been extensively characterized [2]. Attempts in humans, on the contrary, have often focused on *cortical* network nodes using *correlative* neuroimaging approaches, such as task-related activation mapping or brain-wide association studies [17]. In the context of clinical symptoms and their effective treatment, however, these techniques lack insight into the exact *nature* of a given structure-(dys)function relationship: the identified networks can either play a *causative*, *compensatory*, or *epiphenomenal* role [18,19]. Due to this 'causality gap', the effects of an intervention addressing brain correlates established by these methods remain unpredictable [20].

By contrast, emerging network mapping strategies seeding from invasive or noninvasive brain stimulation targets allow for insights into *therapeutic networks* that, by their previous involvement in treatment success, promise a fruitful translation into anatomically targeted neuromodulation therapies [19,21]. Stated simply, mapping a circuit that mediated symptom relief via a *causal* intervention represents the most direct way to inform future neuromodulation targets to treat exactly this symptom [20]. Beyond their undisputable clinical benefit, neuromodulation approaches also increasingly contribute to our understanding of brain functions by matching clinical effects with neuroanatomy across disorders [19,21,22]. One particularly promising method is DBS, which applies highly focal and effective stimulation to subcortical targets that propagates throughout the brain via far-reaching networks [23,24].

A systematic exploration of fronto-subthalamic projections using DBS may shed light onto the longstanding paradox of how stimulation of small brain structures such as the STN can be therapeutic across syndromes as phenotypically diverse as PD [10] or OCD [13]. A similarly puzzling paradox is that brain stimulation to different targets – such as DBS of the STN vs. the internal pallidum (GPi) in PD [25], DYT [26], or TS [27] – can be comparably effective in treating the same disorder. Concurrently, noninvasive stimulation to spatially more extensive cortical sites entails benefit for equivalent functional domains [28,29]. These counter-intuitive results can be conclusively

reframed by conceptualizing different targets as nodes of access to the same circuitry that can be modulated to unfold a given therapeutic effect [27,29–32].

The above observations further imply that the functional role of anatomical subterritories within these hubs must – to some degree – remain conserved from cortical (range of *centimeters*, 10-100 million neurons) toward subcortical network hubs (*millimeters*, 10-100 thousand neurons) – albeit in a spatially miniaturized form. In other words, the functional topography of cortical areas is likely reflected within the topography of their projections within the STN [2,3]. This view is supported by models of a cortico-subcortical funneling architecture, with the basal ganglia acting as a dimensionality reduction or information convergence system [33].

Based on this rationale, herein, we identify optimal connectivity profiles and subthalamic stimulation sites of effective DBS electrodes targeting the STN in four different brain disorders (PD, DYT, OCD, or TS). By these means, we establish a segregation of the frontal cortex and STN into disease-relevant functional domains with causal implications.

Results

Patient Demographics and Clinical Results

Each of the four disorders was represented by two international cohorts of bilaterally implanted STN-DBS patients (N = 197, 394 DBS electrodes): DYT (N = 70, 38 female), PD (N = 94, 29 female), OCD (N = 19, 10 female), and TS (N = 14, 3 female). Relative average improvements from DBS ON to baseline were comparable between cohorts and centers. In DYT, the *San Francisco* cohort presented with an average improvement of 52 ± 42% and the *Shanghai* cohort of 65 ± 29% on the motor subscale of the Burke-Fahn-Marsden Dystonia Rating Scale (BFMDRS). Patients in the TS cohort from *Pisa/Milan* benefitted by 62 ± 18% and those from *Shanghai* by 62 ± 26% within the Yale Global Tic Severity Scale (YGTSS). In PD, the *Berlin* cohort improved by 45 ± 23% and the *Würzburg* cohort by 49 ± 24% on the Unified Parkinson's Disease Rating Scale – Part III (UPDRS-III). DBS entailed a 45 ± 29% reduction within the Yale-Brown Obsessive-Compulsive Scale (Y-BOCS) for the OCD cohort from *London*, while *Grenoble* patients improved by 44 ± 32%. Further demographic and clinical patient characteristics along with DBS and imaging specifications are summarized in **Table S1**. **Tables S2-5** provide comprehensive patient-specific information.

Disease-wise cohorts were analyzed separately but each underwent equivalent processing steps (**Fig. 1**). Electrode localization via Lead-DBS software, v3.0 (www.lead-dbs.org) [34] confirmed placement to the subthalamic region for all patients (**Fig. 2**). Electric field magnitudes (E-fields) estimated based on patient-specific stimulation parameters were used to determine optimal stimulation targets (*DBS Sweet Spot Mapping*, **Fig. 1a**) as well as tracts (*DBS Fiber Filtering*, **Fig. 1b**) that correlated with maximal symptom improvements. Fiber tracts were

primarily defined based on a normative ultra-high-resolution (760 µm isotropic) tractogram of a single healthy participant [35] to identify small differences in anatomical mappings but repeated using three additional normative connectomes. These included a group connectome [30] representative of average connectivity in a large healthy human sample [36], the Basal Ganglia Pathway Atlas [37] to circumvent tractography-based limitations [38], as well as a customized pathway atlas (DBS Tractography Atlas, v2) created by population-based fiber tracking combined with information from different pathway atlases [37,39] with explicit focus on cortico-subthalamic inputs not represented in other atlas resources (see supplementary methods).

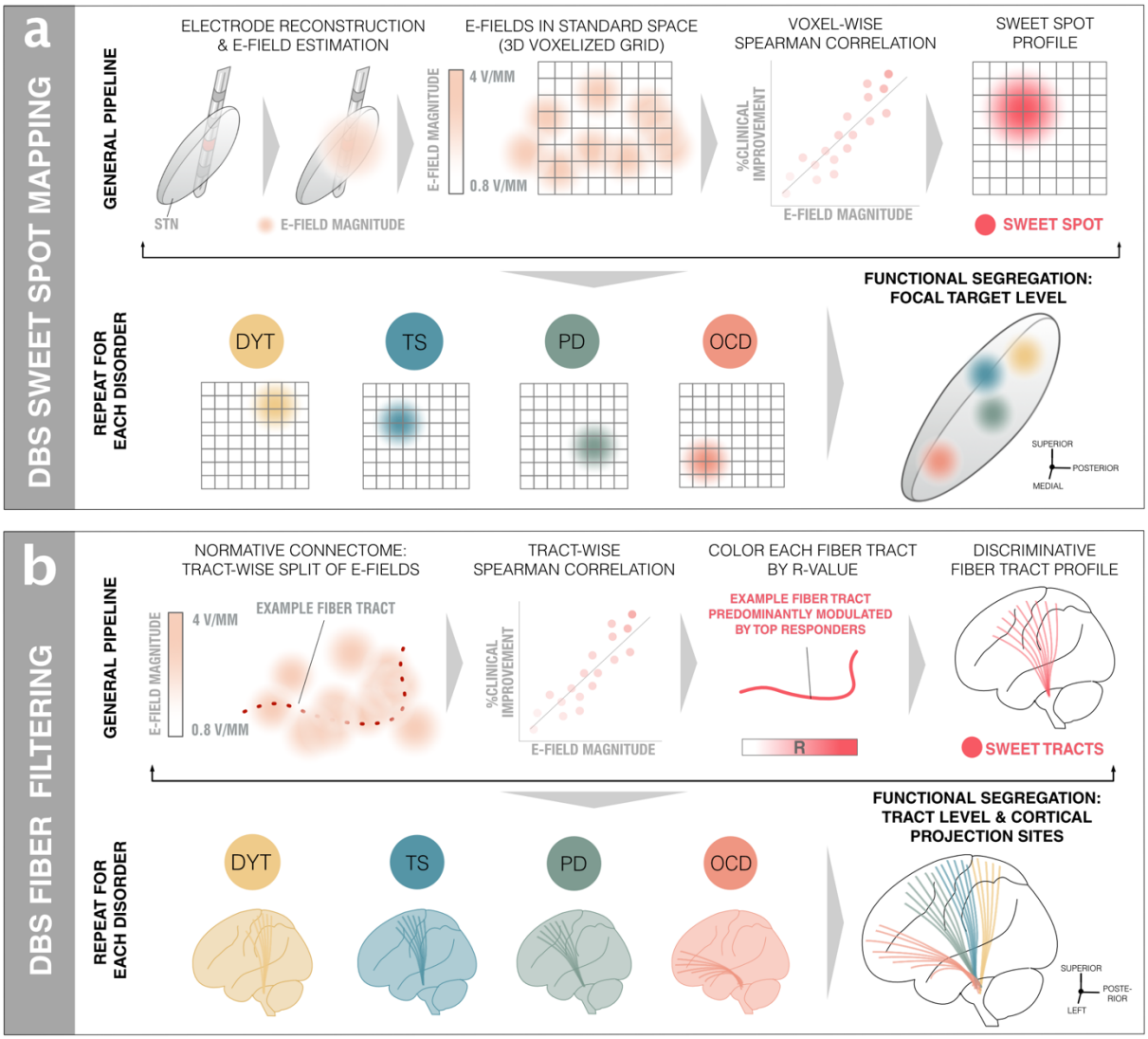

Fig. 1: Overview of the two-fold group-level approach to derive (sub)cortical functional topography. a) *DBS Sweet Spot Mapping*. Using Lead-DBS software, v3.0 [40], patient-specific electrode reconstructions were first derived relative to their precise position within the subthalamic nucleus (STN) region and integrated with individual stimulation parameters to estimate electric field magnitudes (E-fields). Subsequently, disease-wise rank-correlations between E-field magnitudes of the vector and clinical improvements were performed. Applying this procedure across voxels resulted in a detailed grid of positively (sweet spot) and negatively (sour spot, not shown here) associated stimulation sites. **b)** *DBS Fiber Filtering*. Per disease cohort, each tract within a predefined normative connectome was weighted

by its ability to discern good from poor responders. To do so, peak E-field magnitudes among samples drawn along the anatomic course of each tract were rank-correlated with clinical outcomes. Tracts predominantly modulated by high E-field magnitudes of good responders received high positive weights (sweet tracts) – or high negative ones in case of poor responders (sour tracts, not shown here).

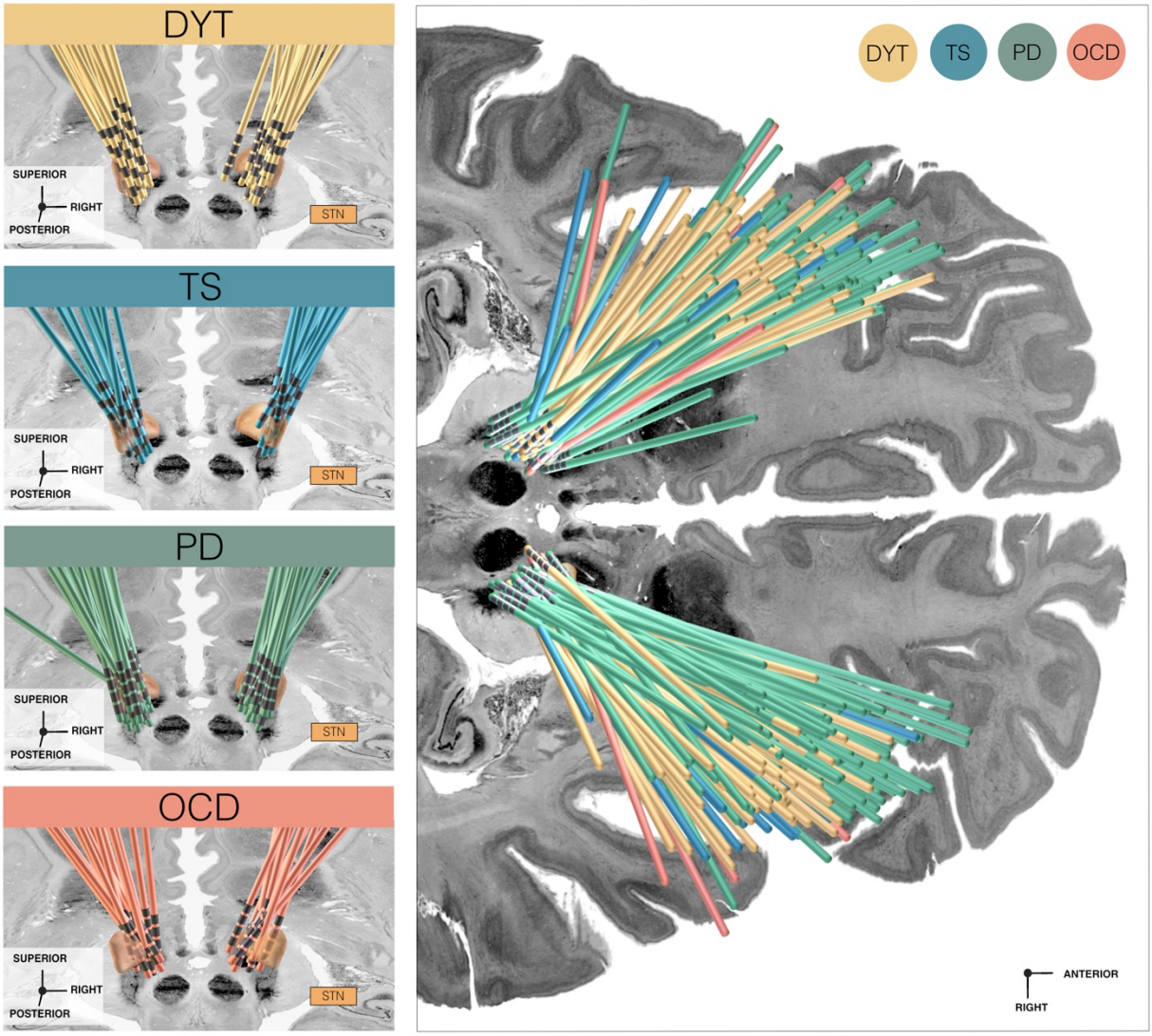

Fig. 2: Overview of electrode placements relative to the subthalamic nucleus across disease cohorts. Deep brain stimulation (DBS) electrode placement as derived using Lead-DBS software, v3.0 [40] is shown in relation to a posterior view of the subthalamic nucleus (STN) in dystonia (DYT), Parkinson's disease (PD), Tourette's syndrome (TS) and obsessive-compulsive disorder (OCD) cohorts, respectively (left panel), as well in an upper axial view of all disorders in conjunction with each other (right panel). STN defined by the DBS Intrinsic Template (DISTAL) atlas [41], with an axial plane of the BigBrain template in 100 µm resolution [42] displayed as a backdrop (z = -10 mm).

Functional Segregation at the Subthalamic Target Level (*DBS Sweet Spot Mapping*)

Model definition: In the first step of our two-fold analysis stream, disease-wise stimulation effects were mapped into anatomical space at the subthalamic level. To do so, E-Field magnitudes were correlated with clinical improvements on a voxel-by-voxel basis as introduced in Horn et al. [43] (**Fig. 1a**). A caudo-rostral lateral-medial organization emerged for peak voxels associated with beneficial stimulation ranging from DYT to TS, PD, and OCD (**Fig. 3**). This result was consistent with functional zones of the nucleus (DYT in the sensorimotor, TS in the motor, PD in the motor-premotor, and OCD in the associative-limbic domain). For details of the anatomical distribution of sweet and sour spots per disease see **Fig. 3** as well as **Table S6** for peak voxel coordinates.

Estimation of outcomes based on the model: We calculated the amount of variance explained by the sweet spot model (per disorder) by spatially correlating individual E-fields with the optimal pattern **(Fig. 3)**. This analysis was carried out i) to compare results between diseases, and ii) to compare amounts of variance accounted for by sweet spots vs. tracts. Critically, in-sample analyses were circular in nature and should thus not be overinterpreted. Instead, analyses were repeated in a 5-fold cross-validation design (**Fig. 3**) to investigate generalizability of findings, which yielded significant results in all disorders but the TS model (with the lowest N).

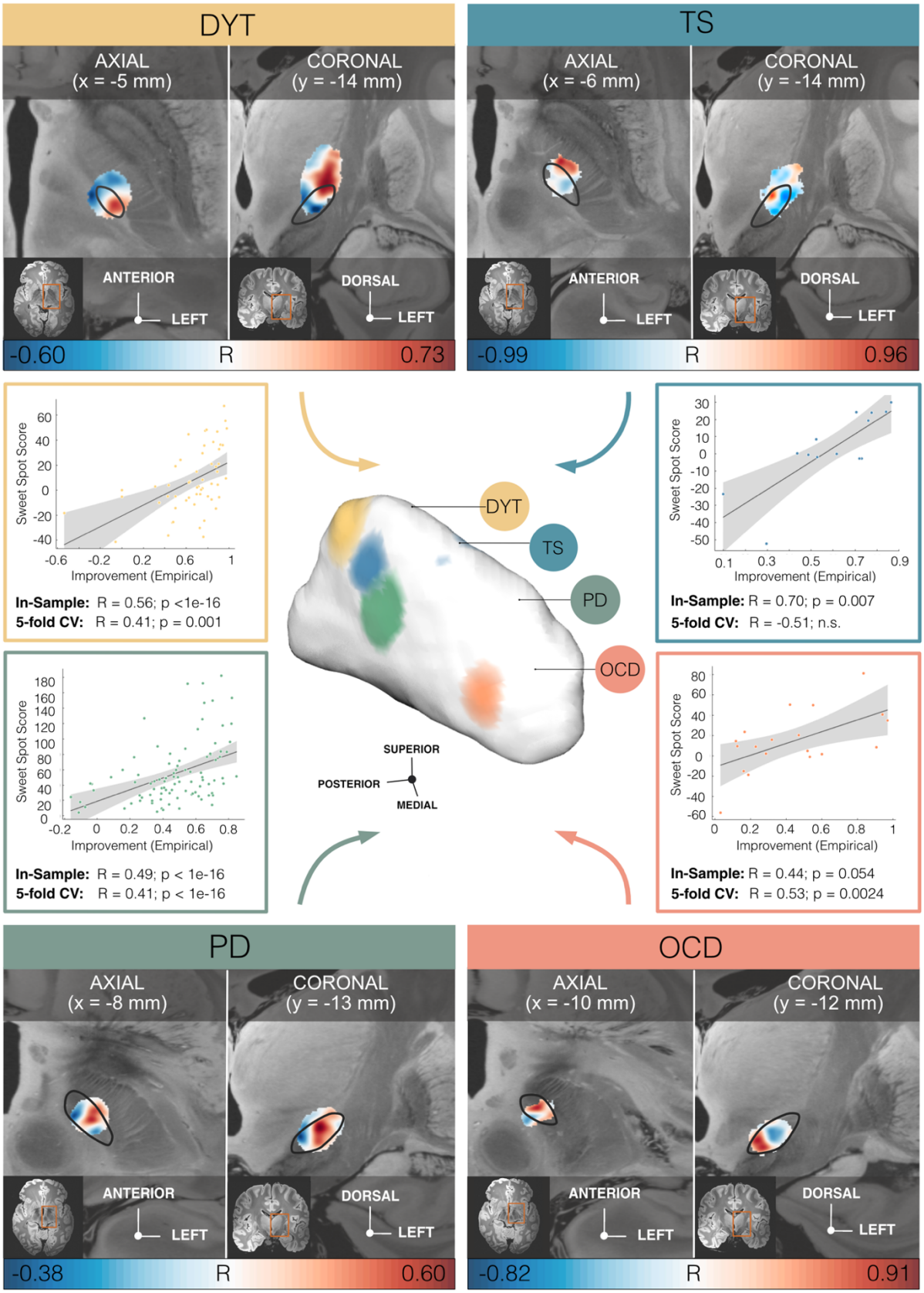

Fig. 3: Functional segregation by disease-specific focal stimulation effects at the subthalamic target level. *Middle panel, center:* Functional gradient of disorder-wise deep brain stimulation (DBS) sweet spots, projected to the surface of a three-dimensional model of the left subthalamic nucleus (STN) in template space derived from the DBS Intrinsic Template (DISTAL) atlas [41]. Binarized and thresholded sweet spot peaks are shown for dystonia (DYT),

Tourette's syndrome (TS), Parkinson's disease (PD), and obsessive-compulsive disorder (OCD). *Upper and lower panels:* Axial and coronal views of disease-wise sweet and sour spots are displayed relative to the left STN (black outlines), superimposed onto an 100 µm ex-vivo template [44]. Voxels are color-coded by correlation strength (warm colors for positive and cool colors for negative associations) between electric field (E-field) magnitudes and clinical improvements. *Middle panel, left and right:* Correlation plots show amounts of clinical outcome variance explained by similarity in E-field peaks with disease-wise models of sweet spots across the cohort, with grey shaded areas representative of 95% confidence intervals. *Abbreviations:* CV, cross-validation.

Functional Segregation at Tract and Cortical Levels (*DBS Fiber Filtering*)

Model definition: In the second step, we mapped optimal stimulation effects to fronto-subcortical circuitry. Specifically, we carried out DBS Fiber Filtering [45] adapted for use in non-binarized E-fields [46] to isolate those streamlines from a normative ultra-high-resolution connectome [35] that are predominantly modulated in top (but not in poor) responding patients. The resulting tract profile represents a model of optimal connections that DBS electrodes should ideally display to maximize treatment benefit [30].

Disease-wise data associated a respectively different tract bundle with optimal improvements (**Fig. 4a & 5**). Beneficial DBS networks for DYT primarily projected from somatosensory (S1) and primary motor (M1) cortices as well as the cerebellum, while predominant electrode connectivity with M1 and supplementary motor areas (SMA) in TS, with premotor regions and SMA in PD, and with ventromedial prefrontal, dorsal anterior cingulate, dorsolateral prefrontal and orbitofrontal cortices in OCD emerged as critical for high stimulation benefit. Peak voxel coordinates of these cortical projections are listed in **Table S6**.

Influence of electrode placement: Importantly, Fiber Filtering results represent tracts *weighted by clinical improvements*, which should not be confused with mere electrode connectivity. Indeed, the DBS implantation site of the standard (second-to-lowest) DBS contact in DYT, PD and TS resided at negligible distance from each other along the y-axis of the STN (p of all comparisons > 0.27) while a significantly different subthalamic aspect was targeted in OCD (all $p < 0.01$). Hence, we hypothesized that results would not merely be driven by *different electrode placement* per disease, but also majorly influenced *by clinical relevance for symptom improvements* of tract stimulations. To investigate this, we overlayed sweet tracts on top of unweighted tracts (i.e., the entirety of tracts that could possibly be isolated based on mere electrode connectivity) in each disease (**Fig. 4a, first row**). As expected, results in all four disorders demonstrated the selectivity of functionally weighted tracts filtered from the wide-spread range of fibers activated by stimulation volumes (**Fig. 4a, second and third rows**).

Estimation of outcomes based on the model: Subsequently, we used optimal tract profiles to estimate clinical improvements of individual patients. Again, we carried out in-sample correlations (for comparisons with sweet spot models and across diseases) and 5-fold cross-validations (to test generalizability) based on optimal fiber models (**Fig. 4b**). Circular models were

significant for all disorders. When subjected to 5-fold cross-validations, the DYT and PD models were robust across all connectomes but less so for disorders comprising smaller sample sizes (TS/OCD). This is not surprising, since 5-fold cross-validations for models calculated on 14 (TS) or 19 (OCD) patients are prone to failure, by design. Robustness of findings from the larger cohorts (PD/DYT), however, make us confident about the general validity of methodological choices. Furthermore, the OCD response tract obtained here has been widely reproduced based on OCD cohorts stimulated at other subcortical targets [30,47,48].

Model specificity: Despite functional segregation, disease-wise sweet tract models – expectedly – also showed considerable overlap, most visibly among TS and PD bundles. To quantify the degree of specificity, each tract profile was hence used to cross-estimate outcomes in all remaining disorders (**Fig. S1**). Tract models were able to explain significant amounts of variance uniquely in the disease for which they had been initially calculated. An exception was seen in case of the TS tract used to estimate PD outcomes – although with a modest correlation.

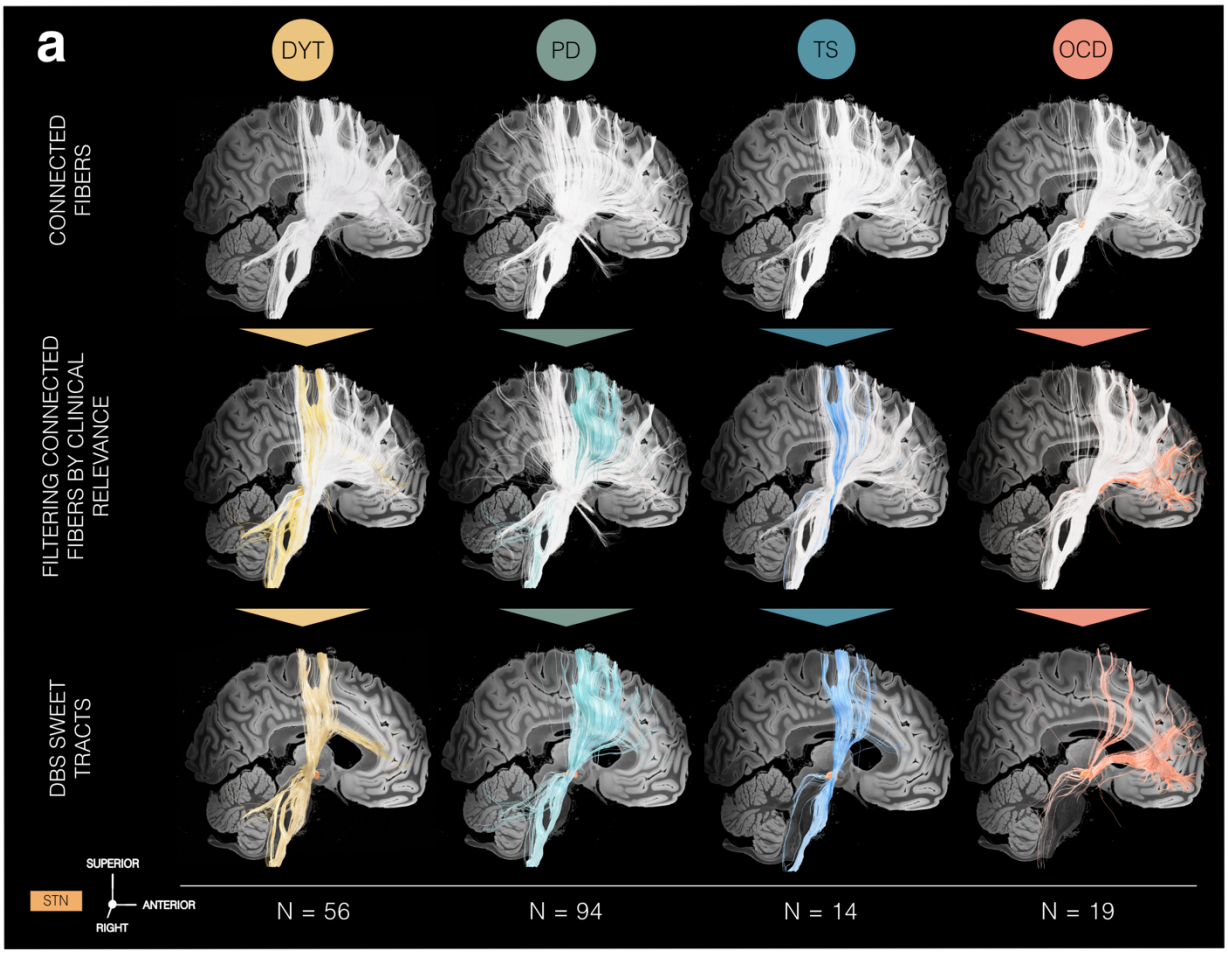

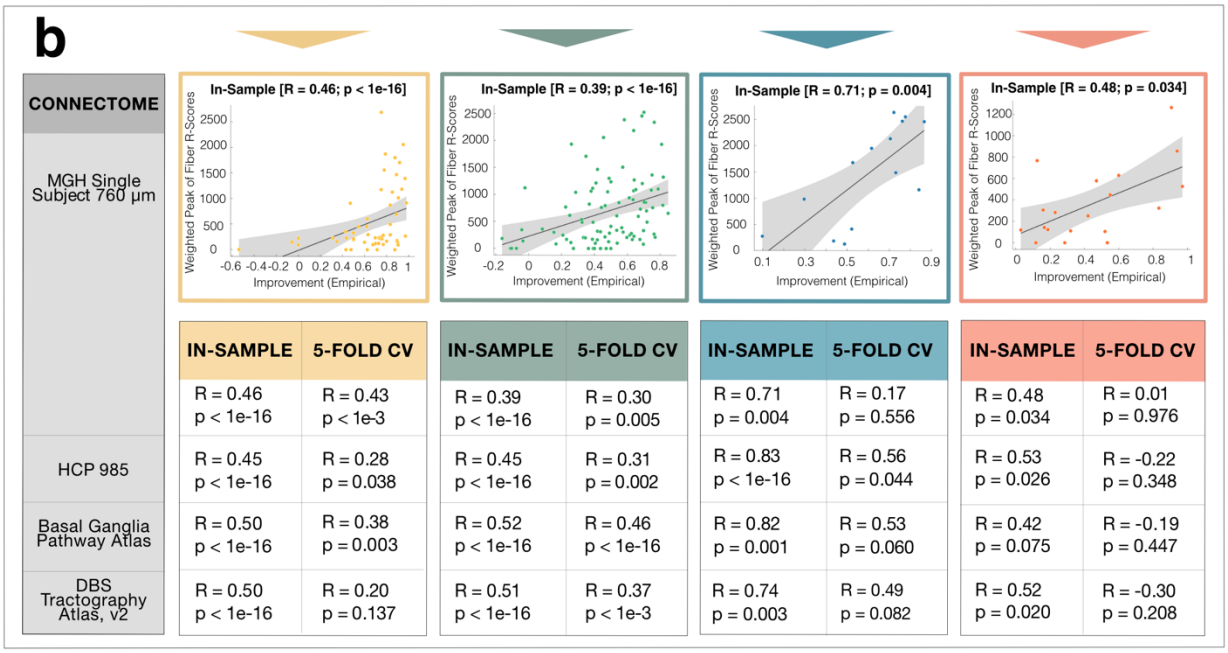

CONNECTOME	IN-SAMPLE	5-FOLD CV	IN-SAMPLE	5-FOLD CV	IN-SAMPLE	5-FOLD CV	IN-SAMPLE	5-FOLD CV
MGH Single Subject 760 µm	R = 0.46 p < 1e-16	R = 0.43 p < 1e-3	R = 0.39 p < 1e-16	R = 0.30 p = 0.005	R = 0.71 p = 0.004	R = 0.17 p = 0.556	R = 0.48 p = 0.034	R = 0.01 p = 0.976
HCP 985	R = 0.45 p < 1e-16	R = 0.28 p = 0.038	R = 0.45 p < 1e-16	R = 0.31 p = 0.002	R = 0.83 p < 1e-16	R = 0.56 p = 0.044	R = 0.53 p = 0.026	R = -0.22 p = 0.348
Basal Ganglia Pathway Atlas	R = 0.50 p < 1e-16	R = 0.38 p = 0.003	R = 0.52 p < 1e-16	R = 0.46 p < 1e-16	R = 0.82 p = 0.001	R = 0.53 p = 0.060	R = 0.42 p = 0.075	R = -0.19 p = 0.447
DBS Tractography Atlas, v2	R = 0.50 p < 1e-16	R = 0.20 p = 0.137	R = 0.51 p < 1e-16	R = 0.37 p < 1e-3	R = 0.74 p = 0.003	R = 0.49 p = 0.082	R = 0.52 p = 0.020	R = -0.30 p = 0.208

Fig. 4: Disease-wise sweet tract models. a) Sweet tracts in dystonia (DYT) (peak R = 0.32), Parkinson's disease (PD) (peak R = 0.35), Tourette's syndrome (TS) (peak R = 0.61) and obsessive-compulsive disorder (OCD) (peak R = 0.42) associated with beneficial stimulation outcome are filtered from an ultra-high-resolution normative connectome [35]. The first row visualizes the set of plain connections (in white) to the group of right-hemispheric stimulation volumes across patients in each of the four disorders in focus. Among all activated streamlines, only those are subsequently singled out by Deep Brain Stimulation (DBS) Fiber Filtering (as highlighted in disease-specific color) which

demonstrate relevance for functional outcome (*second row*). The selectivity of functionally weighted sweet tracts (*third row*) emerging from the wide span of plain connections suggests that functional segregation is not merely driven by differences in electrode positioning between disorders. Instead, it is majorly defined by the importance of modulating this tract for clinical outcome. Results are shown against a sagittal slice (x = -5 mm) of the 7T MRI ex-vivo 100 µm human brain template [44] in conjunction with a 3D model of the right subthalamic nucleus (STN) in template space from the DBS Intrinsic Template (DISTAL) atlas [41]. **b)** In-sample correlations and 5-fold cross-validations (CV) are reported for models informed on four different normative connectomes. Plots in the top row represent the fitting of a linear model to determine the degree to which overlap of electric fields with selected tracts from the Massachusetts General Hospital (MGH) Single Subject 760 µm Connectome explains variance in clinical outcomes across the cohort. Grey shaded areas indicate 95% confidence intervals. *Abbreviation:* HCP, Human Connectome Project.

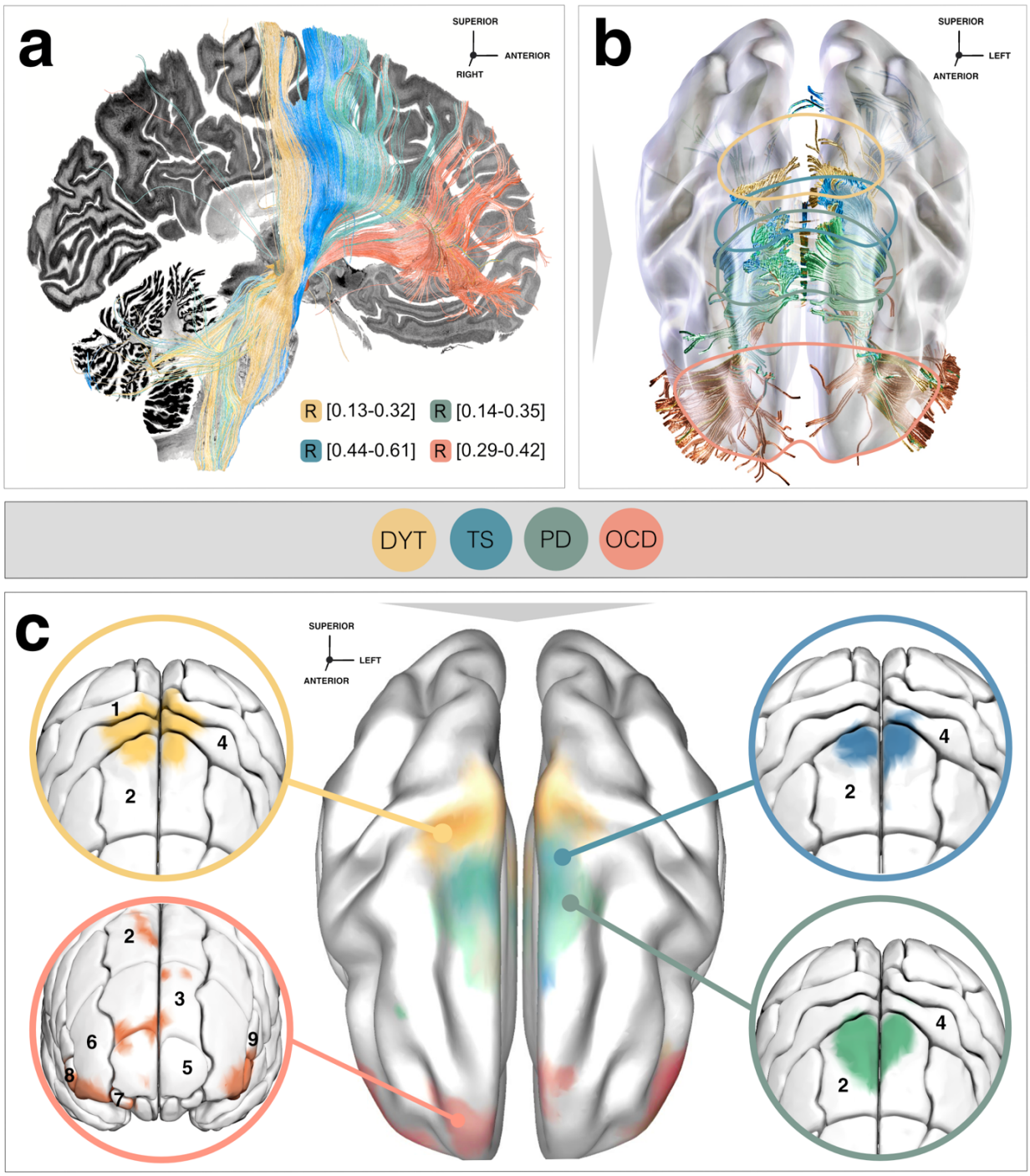

Fig. 5: Functional gradient of fiber tracts and their cortical projection sites associated with therapeutic stimulation effects. a) Functional segregation into therapeutic networks is achieved by means of deep brain stimulation (DBS) Fiber Filtering in dystonia (DYT), Parkinson's disease (PD), Tourette's syndrome (TS) and obsessive-compulsive disorder (OCD). Disease-wise optimal tracts were isolated from an ultra-high-resolution normative connectome [35] through association with clinical effects in each disorder and displayed against a sagittal slice (x = -5 mm) of a brain cytoarchitecture atlas in ICBM 2009b Non-linear Asymmetric ("MNI") space [42]. **b)** Tracts shown in conjunction with a transparent brain in template space along with color-coded delineations. **c)** To derive the cortical gradient of functional specificity, smoothed cortical fiber projections were projected onto a template in MNI space. Zoom-in circles show disease-wise projection sites, as characterized by the Johns Hopkins University (JHU) atlas parcellation [49]. Legend of relevant regions containing fiber projections, with respective JHU atlas denominators in brackets: 1 (JHU: 23 & 24), *postcentral gyrus*; 2 (JHU: 1 & 2), *superior frontal gyrus (posterior segment);* 3 (JHU: 3

& 4), *superior frontal gyrus (prefrontal cortex);* 4 (JHU: 25 & 26), *precentral gyrus;* 5 (JHU: 5 & 6), *superior frontal gyrus (frontal pole);* 6 (JHU: 9 & 10), *middle frontal gyrus (dorsal prefrontal cortex);* 7 (JHU: 17 & 18), *lateral fronto-orbital gyrus;* 8 (JHU: 13 & 14), *inferior frontal gyrus pars orbitalis;* 9 (JHU: 15 & 16), *inferior frontal gyrus pars triangularis.*

Influence of connectome. While main analyses were informed on a connectome of unprecedented spatial (760 µm) and angular resolution [35], the choice of connectome may bias results. First, since the Wang connectome is based on a single human brain, we repeated analyses on a group connectome [30] calculated on diffusion-weighted magnetic resonance imaging (dMRI) based tractography of 985 healthy participants of the Human Connectome Project (HCP) [36] representative of average/population brain connectivity (**Fig. 6b**). A key problem of data-driven whole-brain connectomes (such as the Wang/HCP ones) is their proneness to false-*positive* tracts [38] and low accuracy in representing small subcortical tracts [50]. To account for this, we repeated our analysis on a pathway atlas manually curated by expert anatomists [37] (**Fig. 6c**). While this dataset is likely the most accurate atlas of subcortical tracts that currently exists, a potential drawback is its proneness to false *negatives* (simply because not all fibers of the brain were defined in it). Second, as the atlas is not based on empirical dMRI, small details of tract trajectories in template space may be misaligned. Thus, we replicated analyses using a pathway atlas informed on population based fiber tracking with expert defined pathways [37,39] which we augmented by inputs to the STN from the entire frontal cortex (DBS Tractography Atlas, v2, **Fig. 6d**). Despite clear differences (**Fig. 6**), a comparable rostro-occipital gradient emerged across connectomes, with the same order of motor disorders in sensorimotor and premotor cortices toward associative-limbic OCD connections. In-sample correlations and 5-fold cross-validations of models informed on these connectomes are reported in **Fig. 4b**.

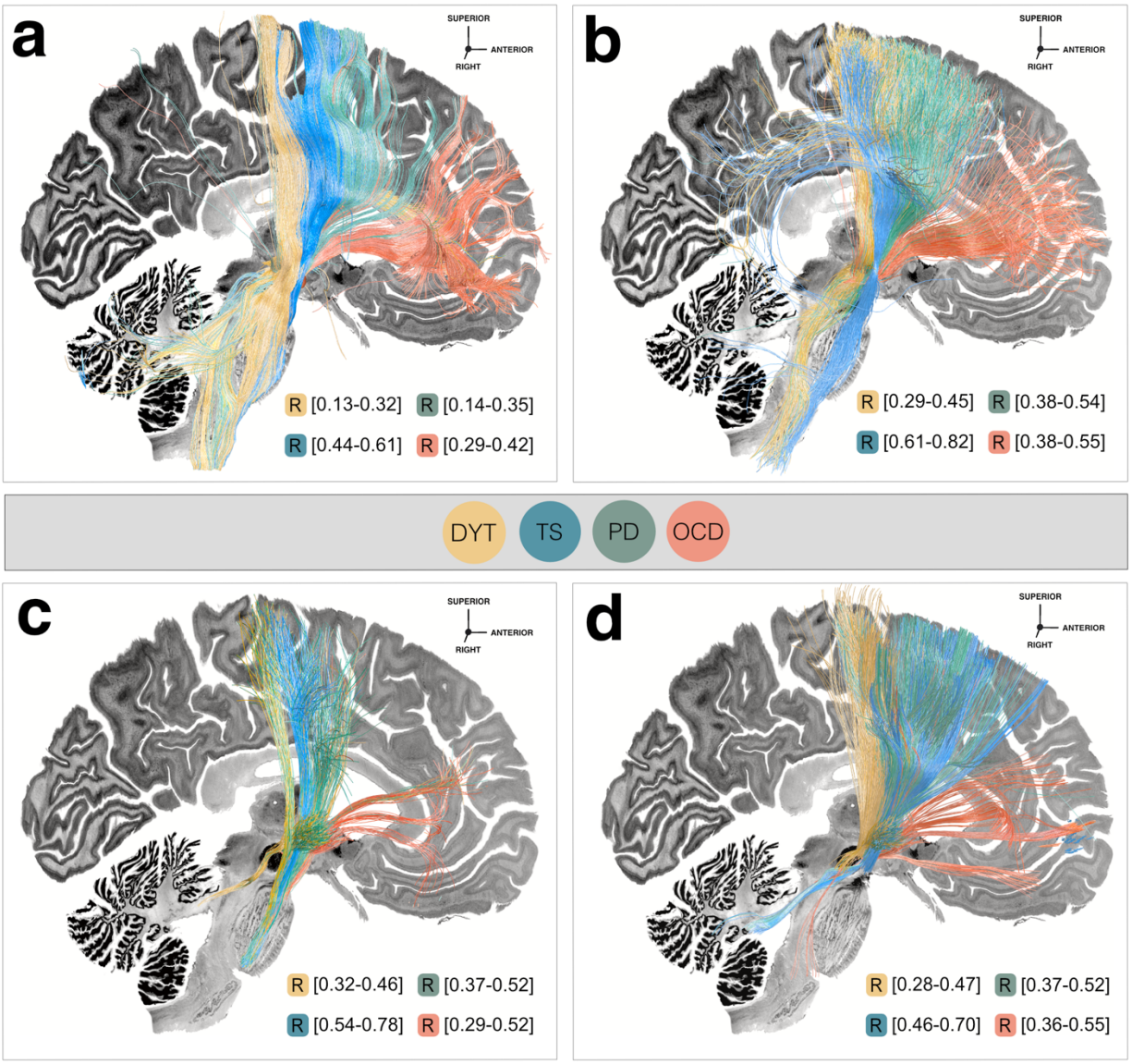

Fig. 6: Influence of the connectome on the functional gradient. To scrutinize the impact of choosing a specific connectomic resource on the topographical organization of functional attributions, we recalculated the disease-wise deep brain stimulation (DBS) Fiber Filtering analysis using four different connectomes. A similar caudo-rostral gradient of functional organization emerged for beneficial fiber bundles filtered from the Massachusetts General Hospital Single Subject 760 µm Connectome [35] **(a)**, the Human Connectome Project (HCP) 985 Connectome [30,36] **(b)**, the Basal Ganglia Pathway Atlas [37] **(c)**, as well as the DBS Tractography Atlas, v2 (see supplementary methods) **(d)**. Results are shown against a sagittal slice (x = -5 mm) of the Big Brain template [42]. *Abbreviations:* DYT, dystonia; OCD, obsessive-compulsive disorder; PD, Parkinson's disease; TS, Tourette's syndrome.

Functional Segregation at the Level of Indirect Pathway Projections

While *hyperdirect* input to the STN is best suited to segregate the frontal cortex, the cortico-basal ganglia-thalamocortical system forms loops including indirect projections from the striatopallidofugal system (and particularly the external pallidum, GPe) to the STN [51]. These latter are thought to converge at the same sites of respective hyperdirect input. Structural representations of the indirect pathway connecting GPe and STN are organized within Edinger's comb system [43,52] and hard if not impossible to reconstruct from dMRI based tractography given their orthogonal course to the highly anisotropic internal capsule [37].

To interrogate the functional organization of indirect connections, we thus repeated our DBS Fiber Filtering analysis based on pallido-subthalamic tracts provided by the Basal Ganglia Pathway Atlas [37]. Again, functional segregation was evident between disease-wise projections and their organization largely consistent with hyperdirect pathway and sweet spot gradients **(Fig. 7)**. An exception emerged in the reversed ordering between TS and PD, pointing toward the complexity of TS (as a neuropsychiatric disease) that may be difficult to resolve further based on the small sample size at hand. While therapeutic indirect connections in DYT projected from sensory/sensorimotor STN regions, those in PD connected to territories within its premotor zone. Finally, TS projections predominantly resided within associative and those of OCD within limbic subthalamic aspects (insets in **Fig. 7**).

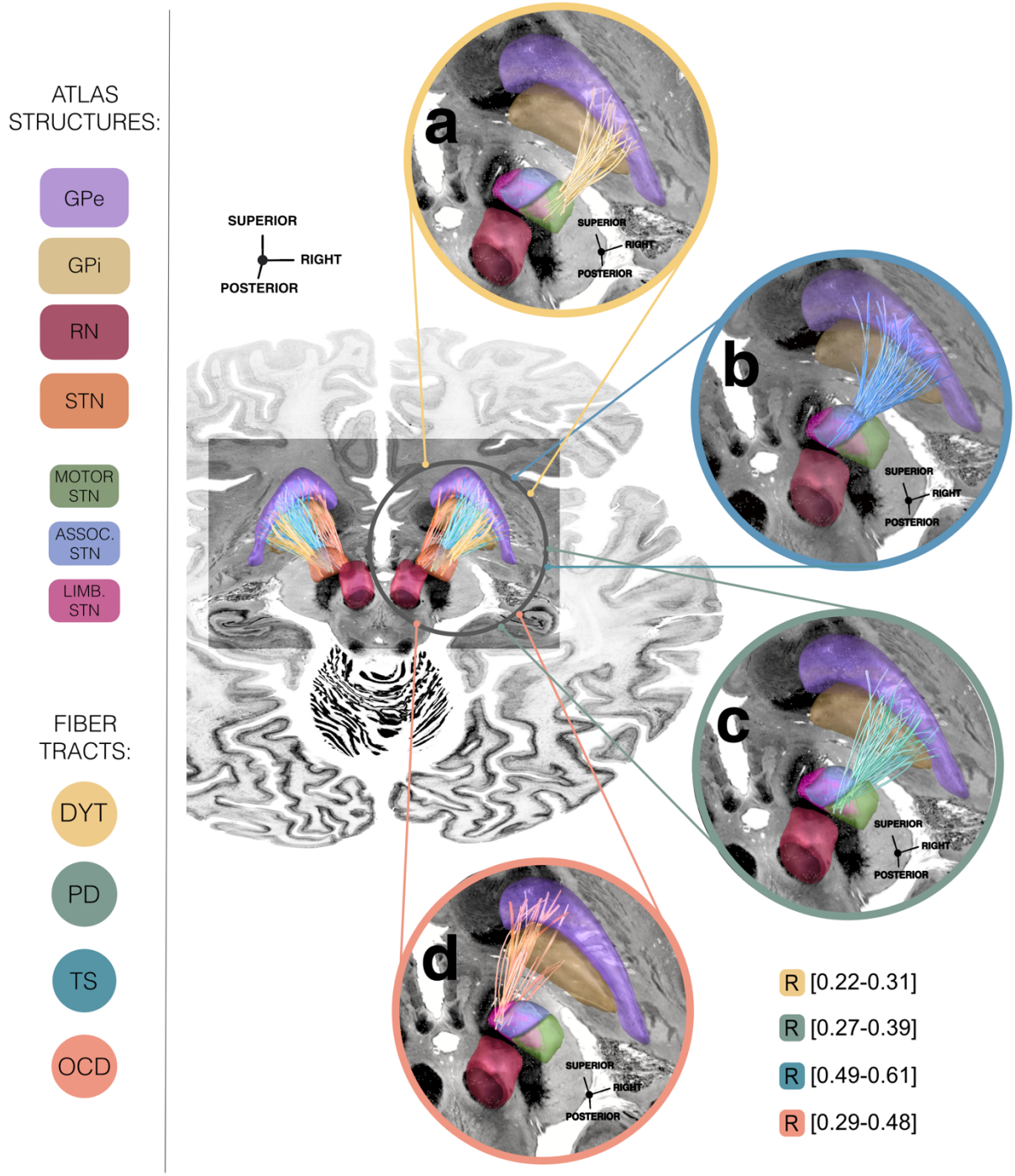

Fig. 7: Conserved functional segregation within *indirect* subthalamic-pallidal connections. Disease-wise sweet tracts – in synergy in the center and separately in close-up views – retain a high degree of functional specificity along their indirect pathway trajectory from the subthalamic nucleus (STN) toward internal (GPi) and external pallidum (GPe). Sweet tracts are informed on an edited version of the Basal Ganglia Pathway Atlas [37] with a focus on subthalamic-pallidal connections. Fibers associated with optimal deep brain stimulation (DBS) outcomes in dystonia (DYT) project from sensorimotor **(a)**, in Tourette's syndrome (TS) from associative **(b)**, in Parkinson's disease (PD) from premotor **(c)**, and in obsessive-compulsive disorder (OCD) from limbic **(d)** STN territories. Fibers are displayed relative to several anatomical structures from the DBS Intrinsic Template (DISTAL) atlas [41] and in conjunction with an axial slice (z = -10 mm) of the BigBrain template [42]. *Abbreviations:* ass. STN, associative territory of the subthalamic nucleus; limb. STN, limbic territory of the subthalamic nucleus; motor STN, motor territory of the subthalamic nucleus; RN, red nucleus.

Spatial Scaling of Functional Representations from Cortex to Subcortex

The basal ganglia *anatomically* compress cortical inputs. During this process, a concurrent compression of *information* is bound to happen [33]. Anatomical projections then re-expand on their way back, via the thalamus, toward the cortex. Within this loop, the STN forms one of the smallest nuclei and receives input from the entire frontal cortex [3]. As such, it embodies a network node with particularly high compression density. In other words, the STN may incorporate a drastically miniaturized representation of how functionally selective anatomy in the frontal cortex is organized.

While the ratio of anatomical scaling carried out by the basal ganglia has been estimated before [53], the present dataset constitutes a unique opportunity to empirically confirm these estimates in the human. Here, we define spatial scaling as the anatomical relationship of distances between pairs of functionally selective cortical vs. subcortical points.

Based on the comparable topography of subthalamic sweet spots and cortical sweet tract projection sites across disorders, we calculated hemisphere-wise distances between all possible combinations of peak coordinates (**Fig. 8**), both at cortical and subcortical levels (**Table S7**). After averaging hemisphere-wise distances, quotients of cortical and subcortical pairs of distances (e.g., A-B and A'-B' in **Fig. 8**) were formed and finally averaged. This resulted in a spatial scaling factor of 10.27 ± 7.72, i.e., *on average*, cortical sites distant to each other by one centimeter would project to subthalamic sites distant to each other by one millimeter. Given the three-dimensional nature of the brain, this compression factor (measured here by point-to-point distances) is likely even larger. However, other factors, such as neuronal densities, also play a role.

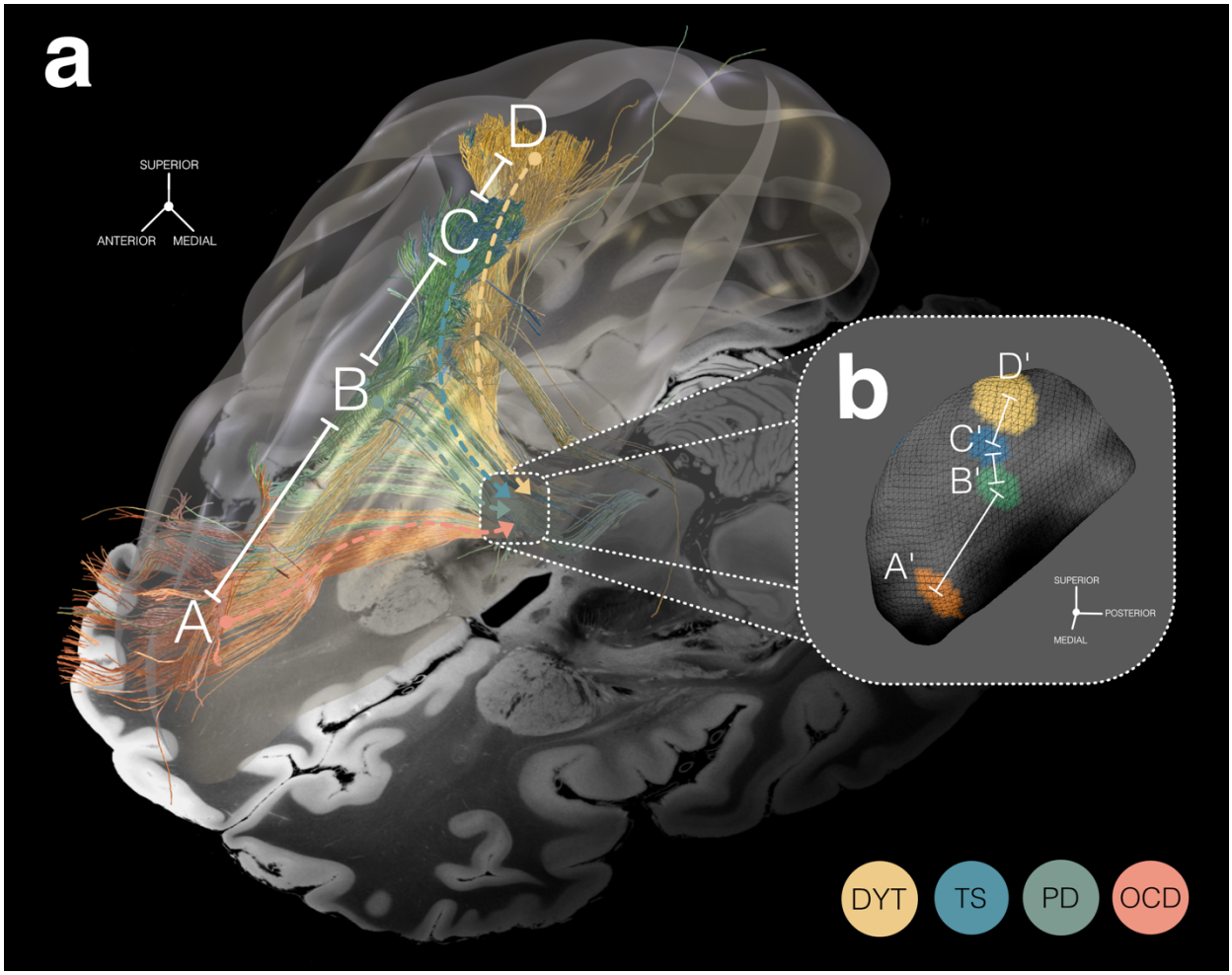

Fig. 8: Spatial compression of functional inputs from the cortex within the subthalamic nucleus. a) Cortical view of functionally selective prefronto-subthalamic tract profiles associated with therapeutic subthalamic nucleus (STN)-deep brain stimulation (DBS) in four disorders – dystonia (DYT), Tourette's syndrome (TS), Parkinson's disease (PD), and obsessive-compulsive disorder (OCD). Axial slice (z = -10 mm) of the 7T MRI ex-vivo 100 µm human brain template [44] displayed as a backdrop, combined with a transparent 3D representation of the right brain hemisphere in ICBM 2009b Non-linear Asymmetric ("MNI") space. **b)** Binarized and thresholded DBS sweet spots are projected to the surface of the right STN (3D model in MNI space from the DBS Intrinsic Template (DISTAL) atlas [41]). **a & b)** Functional segregation by disease-wise stimulation effects can be observed across anatomical analysis levels, in different spatial resolution. While functional domains are organized within the *range of centimeters* at the cortical level, a similar (but miniaturized) gradient is mirrored within the range of *millimeters* at the subthalamic level. Accordingly, fiber tracts with processing preferences for a given functional domain receive input from widespread cortical regions but become more bundled until their projections finally reach the STN, only to re-expand on their way back, towards the cortex. These observations point to a role of the basal ganglia in spatial scaling of functional cortical inputs.

Discussion

Based on 394 invasive stimulation sites in the human STN from eight international cohorts of DYT, PD, TS, or OCD patients, we draw three major conclusions: First, we showcase the network effects of intracranial brain stimulation as a tool to systematically investigate the functional organization of the frontal cortex. Second, DBS allows for *causal inference* regarding couplings between neuroanatomical pathways and clinical dysfunctions. Specifically, beneficial networks for DYT primarily projected from sensorimotor and cerebellar cortices. Predominant electrode connectivity from M1 and SMA in TS, from pre-motor cortex and SMA in PD, and from ventromedial prefrontal, anterior cingulate, dorsolateral prefrontal and orbitofrontal cortices in OCD emerged as essential. Third, mappings of functionally selective stimulation followed a similar topographic organization across neuroanatomical levels: i) among prefronto-subthalamic loops and their cortical projection sites, ii) between external pallidum and STN, and iii) within the STN itself. Comparing cortical to subthalamic functional gradients ultimately allowed to quantify the degree of 'spatial compression' of cortical information within the STN as an example case of the smaller basal ganglia nuclei.

Methodologically, our study demonstrates the use of subcortical neuromodulation combined with connectomics as an effective strategy for probing relationships between neuroanatomy and brain (dys)functions. This concept could be perceived as a network-based extension of historical studies that topographically mapped the sites of direct electrical stimulation (often applied cortically during epilepsy surgery) to specific symptoms. Among the most influential authors, Wilder Penfield and team assembled an exhaustive functional map of the cortex based on intraoperative mapping of sensorimotor phenomena [54]. The present paper inverts this paradigm by combining brain stimulation administered to a specific small (but widely connected) nucleus deep inside the brain with an ultra-high resolution connectome [35]. Demonstrating the utility of this approach could pave the way to similar work in other subcortical and cortical neuromodulation sites.

Conceptually, our results define the functional role of cortico-basal ganglia projections by a *causal* method [19]. The attributions we show were functionally specific, did not merely reflect plain connectivity of differentially placed electrodes (but functional relevance), and could largely be replicated irrespective of which of four connectomes they had been calculated from. Before the teams at Ann Arbor and Johns Hopkins presented their work on what is now referred to as the Albin-DeLong model [6,55], the basal ganglia had been seen as a funnel that integrated information from different cortical strands to the motor cortex which could then initiate action. In other words, the basal ganglia were seen as pure motor structures *before* work by Alexander et al. proposed parallel circuits that involved motor, cognitive and limbic processing [5]. While there is strong cross-communication between these loops at least on cortico-cortical, cortico-striatal, striato-nigral and thalamo-cortical levels, to some degree, the loops remain segregated

throughout their cortico-basal ganglia-thalamo-cortical course [5,56,57]. Subthalamic terminals of direct cortical projections (*hyperdirect pathways*) may best be functionally grouped based on their cortical origin, defining a dorsolateral motor aspect comprising M1 and SMA projections, a ventromedial cognitive territory with origin in superior, middle and inferior prefrontal cortex, and a limbic anteromedial tip with input from orbitofrontal, anterior cingulate and ventromedial prefrontal cortices, hippocampus and amygdala [2,3,41]. Our work confirms the general pattern of this distribution based on invasive stimulation sites in four different brain disorders [19].

Despite segregation between loops, our findings are still compatible with the concept of cross-communication/integration and so-called open-loop architectures [3,4,58]. Indeed, therapeutic targets identified here showed considerable overlap (most notably between TS and PD). In line with the concept of processing *gradients* (rather than entirely segregated loops), our analysis demonstrates *preferential* mappings between anatomy and stimulation effects. This notion also fits with evidence on partial convergence between terminals from different cortical projections sites and interaction between functional subthalamic subterritories [3,59].

Clinically, the identified circuits directly represent therapeutic targets that could inform stereotactic targeting in neurosurgery, and potentially noninvasive neuromodulation at the cortical level [21]. We must emphasize, however, that the degree of certainty varies between the studied disorders given the varying sizes of available samples – especially in TS as a relatively novel application for subthalamic DBS with few patients implanted world-wide to date. In PD, fronto-subthalamic loops connecting the SMA to the STN have been deemed critical in both historical [60] and recent work [61–63]. Structural connectivity between subthalamic electrodes and SMA and pre-motor areas was correlated with motor improvements in PD – and overlap of stimulation volumes with this tract associated with outcomes in independent patients [61]. This is in line with PD motor benefits under cortical SMA stimulation [64]. Functionally, these benefits may relate to involvement of the SMA in movement selection, preparation and initiation [65].

Similarly, sensorimotor and cerebellar loops have been linked to symptom improvements in DYT by investigations that used comparably causal sources of information (such as lesions) [43,66,67]. The sensorimotor cortex along with its basal ganglia projections [68] but also the cerebellum and cerebello-thalamic pathway [69,70] have been related to dystonic pathophysiology, in the past. Concurrently, cortical stimulation of sensorimotor cortex [71] and cerebellum [72] led to clinical benefit. Under DBS, abilities such as motor sequence learning, voluntary movement coordination, sensorimotor adaptation, and the control of specific body parts – which depend on cerebellar or sensorimotor loop function (or an integration of both) [73] – may improve.

In OCD, the tract identified here emerged as an effective 'OCD response tract' beyond stimulation of the STN region [30,45,48]. Most likely conceptualized as an associative-limbic hyperdirect pathway with passage through the internal capsule on its trajectory towards the STN and other mesencephalic nuclei, this bundle receives input from diverse prefronto-cortical regions

such as the anterior cingulate and dorsolateral prefrontal cortex [2,3] – as confirmed via functional mappings [31,48]. Concurrently, these cortical sites have been approved by the US Food and Drug Administration as transcranial neuromodulation targets for OCD [74]. Functionally, recalibrating this tract may resolve repetitive thoughts and behavior by interrupting a pathological control signal emitted through hyperactive prefrontal regions [48,75].

Network correlates to restore functionality in TS are less established, especially not via the more recent application of subthalamic DBS [15,16]. Here, the most highly weighted *hyperdirect* fibers originated in M1 and SMA, which align with tic-related alterations [76,77] and have been associated with tic reduction under thalamic [78,79] or pallidal DBS [27,80]. It is hence not surprising that both M1 and SMA have been probed as noninvasive neuromodulation targets for TS [81]. Functionally, the SMA, in interaction with M1, may be involved in tic preparation, relaying signals to areas underpinning action monitoring or tic execution [82]. Based on the involvement of these regions, effective treatment may facilitate voluntary tic suppression [65], or reduce the premonitory urge to tic [83]. Still, TS – as most if not all basal ganglia disorders – is characterized by a complex amalgamation of affective, cognitive, and somatosensory network aberrations besides motor dysfunctions [77]. While one predominant symptom (e.g., motor tics) may act as a trigger that drives the main network response (expressed as hyperdirect M1 projections), this notion of TS as a neuropsychiatric disorder may explain the here-observed pallido-subthalamic *indirect* projections to the *associative* STN zone.

Concurrently, the above mappings to symptom modulation motivate a quest for the most suitable access node to maximize effects. Although similar functional gradients across anatomical levels may point toward parity between network hubs, one key difference resides in their size. Conserved functional segregation from cortical to subcortical levels implies spatial information downscaling. At microscopic scales, this idea is supported by the anatomical construction of the cortico-striato-pallidal system [33,84]: For instance, cortico-striatal neuron populations (~17 million corticostriatal axons) are estimated to reduce by a factor of ten during striatal integration (~1.7 million striatal projection neurons) [53]. On these grounds, information theoretical accounts have proposed a role of the basal ganglia in dimensionality reduction [33]. The (hyper-)direct cortex-STN connection is ideally suited to analyze this effect (since the STN is among the smallest basal ganglia nuclei). Indeed, its deep placement and dense dendritic arborization position the STN as an optimal hub for access to large-scale brain networks via minuscule electrodes. By contrast, cortical modulation of the same network requires more extensive electrodes or stimulation fields (e.g., as applied by transcranial magnetic stimulation). One downside of this downscaling effect, however, is a loss in specificity: subtle variations in electrode placement may result in larger changes in modulated cortical networks – emphasizing the importance (and difficulty) of precise stereotactic targeting.

Our study should be seen in the light of several limitations. First, analyses relied on retrospective data which may bias the interpretation of clinical outcomes. Assemblage of a large multi-center sample (N = 394 electrodes) further inevitably introduced different sources of variability. Still, the majority of our models extrapolated across differences in targeting strategies between surgeons and centers, imaging modalities and protocols, electrode models, stimulation paradigms, or clinical assessment strategies.

Second, the underlying physiological effect may not be fully captured by the simplified biophysical model employed here to approximate the amount of tissue activated. For instance, E-field models neglect the impact of stimulation onto glial cells, intracellular processes, or synaptic reorganization [85]. Also, different stimulation parameters may entail differential consequences [86]. For these reasons, refined modeling of the focal stimulation impact might contribute to a further increased validity of results [50].

Third, warping lead localizations into template space may have introduced slight mismatches. We sought to counteract this bias as much as possible by use of an advanced processing pipeline which included brain shift correction [34], multispectral normalization, subcortical refinements, and phantom-validated electrode reconstructions [87]. We further applied a normalization strategy with comparable performance in STN segmentation as manual delineations by anatomical experts in two independent evaluations [88,89]. In addition to meticulous visual inspection and refinement of outputs, the subthalamic atlas fit was manually optimized via the WarpDrive toolbox [40].

Fourth, with patient-specific dMRI largely unavailable, anatomical delineations were based on normative connectivity. Undoubtedly, the use of connectivity acquired outside of the patient sample in question introduces limitations regarding the anatomical accuracy of results. Nevertheless, an advantage of the normative connectome principally used here lies in its ultra-high resolution and excellent signal-to-noise-ratio. This unprecedented quality resulted from a long scanning duration and use of advanced acquisition hard- and software [35], which is hardly attainable during clinical imaging. Additionally, we replicated our findings with four normative connectomes to probe for differences as a function of dataset. Indeed, our study aimed to derive at a “broad lens” description of functional networks in the *average human brain*. Instead, patient- or disease-specific connectivity estimates would be biased toward the individual/disease. It could also make a direct comparison of results less straightforward and, importantly, less translatable across DBS indications. Although normative network models could account for significant amounts of variance in clinical improvements outside of the training sample [30,31,46,61], the reported tracts should not be used for targeting before sufficient validation in patient-specific data.

In conclusion, our study demonstrates the potentials of invasive brain stimulation as a causal *"flashlight"* pointing from the subcortex onto the functional organization of the frontal cortex. We found a topographical gradient of beneficial stimulation effects as a function of symptom domain at the level of prefronto-subthalamic circuits and their cortical projection sites, which was mirrored within the subcortex – in downsized fashion. This scaling effect on functional attributions across neuroanatomical levels delivers an empirical basis for a subthalamic role in information compression. It also provides a compelling answer to the conundrum of similar functional effects following stimulation to different access nodes of a shared therapeutic network.

Methods

Patient Cohorts, Imaging, and Clinical Assessments

Data of eight patient cohorts (N = 197) from seven international DBS centers (*San Francisco, Shanghai, Berlin, Würzburg, Grenoble, London*, and *Pisa/Milan*) was included into this retrospective study, each implanted with DBS electrodes to the STN bilaterally for treatment of either DYT (N = 70), PD (N = 94), TS (N = 14), or OCD (N = 19). The full sample consisted of two cohorts per disease, with the *Shanghai* center contributing two cohorts (DYT and TS data). Procedures of all clinical trials and studies (**Table S1**) leading to the collection of these data were carried out according to the declaration of Helsinki from 1975 and all participants signed an informed consent prior to study participation. Post-hoc analyses performed for the purpose of the present manuscript were approved by the institutional review board of Charité – Universitätsmedizin Berlin (master vote EA2/186/18) and treatment of data complied with all relevant ethical regulations.

To inform surgical planning and for exclusion of structural abnormalities, all patients received high-resolution multispectral structural MRI that had been acquired at 3 Tesla field strength. High imaging quality was ensured through visual inspection by a multidisciplinary team during stereotactic planning, and in case of movement artifacts, preoperative acquisitions were repeated under general anesthesia. Intraoperative microelectrode recordings and macrostimulations as well as either postoperative computed tomography (CT) of the head (N = 73) or MRI (N = 124) (**Tables S1 & S2-5**) were acquired to confirm accurate lead placement.

Specifics on electrode models implanted in each cohort are summarized in **Table S1**. Stimulation settings for all cohorts were selected from times of follow-up to which stimulation effects had sufficiently stabilized (**Table S1**). Above and beyond bilateral implantation of DBS electrodes to the anteromedial STN, OCD patients in the London cohort had received an additional set of electrodes targeting the ventral capsule/ventral striatum that were, however, not considered in the present investigation [90]. For this cohort, different stimulation settings with "optimized" stimulation of both targets combined or of each target separately were available. In

the present study, stimulation parameters and corresponding Y-BOCS improvement values collected during the "optimized STN-DBS only" phase were used.

Further, times of follow-up available for some patients within the N = 58 cohort of DYT patients from Shanghai were shorter than those of other disease cohorts. In addition, as DYT is a heterogeneous disease of several forms (e.g., generalized, segmental and focal somatotopic expressions), preoperative BFMDRS summary scores in some Shanghai patients were considerably lower than those of patients in the San Francisco cohort. To ascertain stabilized and comparable DBS effects across cohorts, main analyses were thus carried out on the DYT sample including a subcohort of Shanghai patients (N = 44) which sufficed to more conservative inclusion criteria (baseline BFMDRS scores ≥ 5 and follow-up ≥ 6 months). However, we repeated our results on the complete DYT sample (N = 70) including the full Shanghai cohort (N = 58) to demonstrate stability of effects (**Fig. S2**).

Clinical improvement was measured via relative change from preoperative baseline to postoperative follow-up under DBS ON (or from postoperative OFF to ON DBS conditions in the case of PD) within the primary outcome assessment of each disease cohort: BFMDRS in DYT, UPDRS-III in PD, Y-BOCS in OCD, and YGTSS in TS.

DBS Electrode Localization and Electric Field Modeling

DBS electrodes of all patients were localized based on default settings in an advanced, state-of-the-art processing pipeline as implemented in Lead-DBS software, v3.0 (https://www.lead-dbs.org) [40]. Lead-DBS being a MATLAB based software, MATLAB R2022b, v9.13.0.2105380 (The MathWorks Inc., Natick, MA, USA) was used to implement this analysis pipeline. In brief, our approach involved linear coregistrations of postoperative head CT or MRI scans to preoperative T1-weighted images by means of Advanced Normalization Tools (ANTs, http://stnava.github.io/ANTs/) [91]. Coregistration results were subsequently corrected for potential intraoperative brain shift via an automatized subcortical refinement module (as implemented in Lead-DBS), but also needed to conform to meticulous visual inspection by two expert users (BH and NL). This latter step led to manual refinement in cases where aberrations were detected.

All preoperative acquisitions were used for multispectral spatial normalization into ICBM 2009b Non-linear Asymmetric ("MNI") template space [92] using the Symmetric Normalization (SyN) approach included in ANTs with the "effective: low variance + subcortical refinement" preset in Lead-DBS. This method had outperformed comparable approaches for subcortical normalizations (including STN segmentation) across >10,000 nonlinear warps and different normalization techniques in two independent studies, with precision approaching manual expert segmentation [88,89]. To maximize registration accuracy further, normalization warp-fields were manually refined using the "WarpDrive" tool included in Lead-DBS [40], with particular attention to the STN as the anatomical structure in focus. Across analyses and visualizations of results, atlas

definitions of the STN were based on the DBS Intrinsic Template (DISTAL) atlas [41], a precise subcortical atlas explicitly created for use within Lead-DBS and based on convergent information from multimodal MRI, histology as well as structural connectivity.

Subsequently, electrodes were pre-localized using the phantom-validated Precise and Convenient Electrode Reconstruction for Deep Brain Stimulation (PaCER) algorithm [87] in case of postoperative head CT. In case of postoperative MRI, the trajectory search/contact reconstructions (TRAC/CORE) algorithm [93] was applied instead. The resulting pre-localizations were visually inspected and manually refined by two expert users (BH and NL).

Integrating patient-specific active electrode contacts with stimulation parameters, the electric field (E-field) as the gradient distribution of electrical potential in space was simulated in native patient space via an adaptation of the SimBio/FieldTrip pipeline (https://www.mrt.uni-jena.de/simbio/; http://fieldtriptoolbox.org/) [94] as implemented in Lead-DBS [40]. Using a finite element (FEM) approach, a volume conductor model was created on the basis of a four-compartment mesh [34], which involves a realistic 3D model of electrodes (metal and insulating electrode aspects) and surrounding anatomy (gray and white matter). Again, gray matter was defined using the DISTAL atlas [41]. Finally, electrodes and E-fields were transformed into template space based on the manually optimized warp-fields priorly determined during normalization of preoperative MRI acquisitions. These steps allowed for visualization and analysis of electrodes and stimulation fields at the group-level using the Lead-Group toolbox [62] as well as DBS Sweet Spot and Fiber Filtering explorers [40].

Functional Segregation at the Focal Target Level (*DBS Sweet Spot Mapping*)

*Model definition (**Fig. 1a**):* Our group-level approach intended to delineate and compare the functional organization of disorder-specific stimulation effects across different neuroanatomical levels, namely i) that of the subthalamic target site (*DBS Sweet Spot Mapping*), as well as ii) that of prefronto-subthalamic pathways and their cortical projection sites (*DBS Fiber Filtering*).

In the first part of our analysis stream, DBS Sweet Spot Mapping [43] (**Fig. 1a**) was performed in each disease cohort separately to identify subthalamic voxels related to optimal stimulation effects within each respective clinical outcome measure (i.e., BFMDRS in DYT, UPDRS-III in PD, YGTSS in TS, and Y-BOCS in OCD). Only voxels covered by at least 50% of E-fields with a magnitude above 200 V/m (corresponding to a commonly assumed estimate of voltage needed to activate axons) were considered to account for different numbers of voxels covered among E-fields. Across voxels encompassed by the group of thresholded E-fields in template space, Spearman's rank correlations were calculated between E-field magnitudes and relative clinical improvements. This procedure resulted in a map of positive peak voxels associated with beneficial stimulation effects (*sweet spot*), as well as negative peak voxels related to detrimental effects (*sour spot*). Of note, these correlation coefficients should not be

interpreted as significant results due to the mass-univariate (voxel-wise) nature of our analysis stream. Instead, they were validated by probing model performance in estimating clinical outcomes in a 5-fold cross-validation design (see below).

Estimation of outcomes based on the model: To quantify the capability of each disease-wise sweet spot map in estimating clinical improvements, individual E-fields were multiplied with the model in a voxel-wise fashion and results averaged across voxels. E-fields in which peaks spatially overlapped with the sweet spot would result in estimates of good performance, while overlaps with the sour spot would lead to the opposite pattern (i.e., low or negative estimates). While in-sample correlation results represent circular outcomes, they served the purpose of comparison of results i) across disorders, and ii) between sweet spot and sweet tract findings. Moreover, we tested whether models were robust in a 5-fold cross-validation design to probe generalizability of results. Across analyses, p-values were derived based on permuted testing building on 5,000 iterations.

Visualizations and functional gradient: To visualize the organizational pattern of the functional gradient across disorders within the STN, disease-wise sweet spots were smoothed by a kernel of two at full width at half maximum using Statistical Parametric Mapping (SPM12) software (https://www.fil.ion.ucl.ac.uk/spm/). Smoothed profiles were subsequently projected onto the surface of a 3D model of the STN in ICBM 2009b Non-linear Asymmetric space derived from the DISTAL atlas [41] using SurfIce software, v.1.0.20211006 (https://www.nitrc.org/projects/surfice). Sweet in conjunction with sour spots were additionally displayed separately for each disorder using 3D Slicer software, v5.2.1 (https://www.slicer.org/).

Functional Segregation at Tract and Cortical Levels (*DBS Fiber Filtering*)

*Model definition (**Fig. 1b**):* The second part of our analysis stream followed the intention of deriving the organization of neuroanatomy-function pairings i) at the level of *hyperdirect* prefronto-subthalamic tracts, but also ii) that of their projection sites within the frontal cortex.

To understand the relationship between modulation of specific fiber tracts seeding from bilateral E-fields and a given functional effect, we thus employed a previously validated structural connectivity analysis, termed DBS Fiber Filtering [45] (**Fig. 1b**), in an adapted form for implementation in (non-binarized) E-fields [46]. Structural connectivity was primarily defined by a normative whole-brain connectome, derived from a multi-shell diffusion-weighted imaging dataset at 760 µm isotropic diffusion acquired in-vivo in a single healthy participant over a total duration of 18 scanning hours (Massachusetts General Hospital [MGH] Single Subject 760 µm Connectome) [35]. While by design, normative connectivity is unable to fully account for patient-specific anatomical variability, it is optimally suited for “broad-lens” insights into the average human brain at particularly high resolution as aimed at in the present investigation.

Again, the fiber tract modeling procedure was performed in each disease cohort separately. The first step comprised an estimation of the stimulation impact per E-field on each tract (in a tract-by-tract fashion). To do so, we first isolated such tracts that passed in proximity of at least a small number of electrodes from the total set of five million tracts defined within the normative connectome. These were operationalized in the form of tracts passing through a rather high E-field magnitude (> 0.8 V/mm) in more than 0.5% of E-fields and used to ascertain that tracts were modulated by at least a minimal number of electrodes. Subsequently, for each tract, the peak value among the E-field magnitudes collected from points along its passage was denoted. This resulted in a "tract by E-field peaks" matrix in which each entry denoted the peak impact of each E-field on each tract.

The second step aimed at weighting activated tracts by their correlation with (i.e., relevance for) clinical outcomes. For this purpose, the entries of this matrix were Spearman's rank correlated with clinical improvements across the disease cohort. Following this procedure, each tract was tagged by an R-value coding for its correlation with beneficial stimulation effects. The resulting tract profile can be seen as a model of optimal connectivity for maximal clinical improvements, where tracts with positive weights would be strongly modulated by E-fields of good performers (*sweet tracts*) and such with negative weights by E-fields of poor performers (*sour tracts*). As these correlation coefficients relied on a mass-univariate approach, fiber profiles were later validated by probing their capability to estimate clinical improvement in unseen data (see below).

Estimation of outcomes based on the model: To determine how well the optimal sweet tract profiles would perform in estimating clinical improvement in single patients, the peaks of their E-fields were Spearman's rank correlated with the tract model of optimal electrode connectivity. Following the logic of this procedure, E-field peaks displaying high overlap with beneficial tracts would receive high clinical scores while those with low overlap with beneficial – or even high overlap with detrimental tracts – would receive low clinical estimates. The top 1% of sweet tracts (based on the cumulative distribution function of R-values of all tracts) were selected for this validation step. In this manner, the ability of fiber models of explaining in-sample variance was scrutinized for comparability of results across diagnostic categories and to those of sweet spots. Ultimately, all models were subjected to cross-validations in a 5-fold design to investigate the generalizability of their explanatory value in hold-out data.

Visualizations and functional gradient: To elucidate the organizational gradient of fiber projections at the prefronto-cortical level, sweet tract bundles were first converted to voxelized images (tract-density maps). The resulting maps were then smoothed using an 8 mm Gaussian kernel at full width half maximum as implemented in SPM12 (https://www.fil.ion.ucl.ac.uk/spm/) and projected onto the cortical surface of the MNI template using SurfIce software, v.1.0.20211006 (https://www.nitrc.org/projects/surfice). Anatomical correlates of disease-wise

projection sites of fiber tracts were then defined based on the Johns Hopkins University (JHU) atlas parcellation [49].

Influence of electrode placement: Subsequently, we aimed to scrutinize the relative impact of different model inputs. Besides the choice of a normative connectome, DBS Fiber Filtering results are mainly determined by two major sources of variability across patients: namely, electrode placement and clinical improvements. However, in three out of the four disorders of interest in the present study (DYT, PD and TS), stereotactic targeting aims at a comparable site within the dorsolateral aspect of the STN, while the OCD target resides more anteromedially. To investigate whether segregation of functional mappings across disorders was not merely driven by different electrode placement, sweet tracts in each disorder were thus overlayed on top of mere electrode connectivity. This latter set of tracts represents the entirety of structural connections activated by a bilateral E-field irrespective of their importance for clinical stimulation impact. Demonstrating that only a subsection of connected tracts is clinically relevant would allow for the conclusion that functional outcome – above and beyond electrode placement – is decisive for functional segregation at the level of disease-wise tracts, as well as that of their cortical projection sites.

Model specificity: Besides validation of each model within the respective disorder that it had been calculated on, we were further interested in the degree of specificity of disease-wise models in their ability of explaining outcome variance. To demonstrate specificity, we used each disorder's model to predict clinical outcome in all remaining three disorders. In the case of specificity of functional mappings, each of the models would show predictive utility uniquely for clinical improvements within the corresponding outcome measure, but not for those of other clinical scales.

Influence of choice of connectome: Further, we aimed to scrutinize the influence imposed by the decision for using a particular normative resource to inform connectivity in our DBS Fiber Filtering analyses. To do so, we repeated modeling and model validation procedures using three additional connectomes based on otherwise equivalent model parameters. The first such resource consisted of a group connectome derived from dMRI based tractography data of 985 healthy participants acquired within the HCP 1,200 subjects release [36]. Details on the calculation procedure of this connectome are reported in Li et al. [30]. Second, an axonal pathway atlas (Basal Ganglia Pathway Atlas) [37] was employed which had been manually defined by expert anatomists, thus makes the inclusion of false-*positive* connections unlikely [37], and further circumvents the drawbacks of dMRI based tractography [38]. Third, we employed a custom-made pathway atlas (DBS Tractography Atlas, v2) informed on previously defined pathway atlases, including the DBS Tractography Atlas, v1 [39] and the aforementioned Basal Ganglia Pathway Atlas [37] which was completed by additional tracts of particular relevance to this work (see supplementary methods).

We created this atlas explicitly for the purpose of the present investigation with a focus on subthalamic fiber inputs that were not delineated in other available atlas resources.

Indirect pathway projections: Besides *hyperdirect* fronto-cortical input, the STN receives indirect projections from the striatopallidofugal system [51]. In second instance, we thus sought to understand how *indirect* anatomical connections would be functionally organized as a function of stimulation impact on disorder-wise core symptom domains. To this end, we appended an additional DBS Fiber Filtering analysis informed on pallido-subthalamic connections that had been extracted from the Basal Ganglia Pathway Atlas [37] while keeping remaining model parameters consistent.

Spatial Scaling of Functional Representations from Cortex to Subcortex

Functional gradients at both cortical and subcortical levels resulted in similar orderings across disorders. Their comparison thus provides an empirical window into the degree of spatial downscaling (or re-inflation) by the STN (as an exemplary case of the smaller basal ganglia nuclei) as implemented in the form of cortico-subthalamic projections. To derive at an empirical estimate of this (two-dimensional/point-to-point) compression factor, distances between each possible recombination of disorder-wise peak voxel coordinates of *subcortical* sweet spots (i.e., distances between OCD and PD, PD and TS, TS and DYT, OCD and TS, PD and DYT, as well as OCD and DYT) were first extracted per brain hemisphere. The same procedure was applied to peak voxel coordinates of *cortical* sweet tract projection sites. At both cortical and subcortical levels, distances were subsequently averaged across hemispheres. Finally, quotients between respectively corresponding cortical and subcortical distances were calculated and averaged to form one single quotient of (two-dimensional) 'spatial downscaling'.

Data availability

Clinical outcome and imaging data cannot be publicly shared as this would compromise patient privacy according to current data protection regulations. It is, however, available from the principal investigators of the collecting sites upon reasonable request within the framework of a data sharing agreement. The sweet tract atlas and sweet spots of all four disorders are openly available within Lead-DBS software (www.lead-dbs.org). Further, the DBS Tractography Atlas, v2 can be openly downloaded via the Lead-DBS knowledge base (https://www.lead-dbs.org/helpsupport/knowledge-base/atlasesresources/normative-connectomes/). The HCP-1,065 diffusion source data [95] used to inform this atlas can be openly accessed via DSI-Studio (https://sites.google.com/a/labsolver.org/brain/diffusion-mri-data/hcp-dmri-data). The following normative resources have been made openly available by the original authors: the MGH 760 µm Connectome [44] (https://datadryad.org/stash/dataset/doi:10.5061/dryad.nzs7h44q2) and the Basal Ganglia Pathway Atlas [37] (https://osf.io/mhd4z/). While a processed version of the HCP

985 Connectome [30] can be requested from the corresponding authors, source data are freely accessible via the repository of the HCP (https://www.humanconnectome.org/study/hcp-young-adult/document/1200-subjects-data-release).

Code availability

The entirety of code used in the analyses presented in this work is openly available within the Lead-DBS environment (https://github.com/leaddbs/leaddbs).

Declaration of Competing Interests

J.L.O. reports research grant support from Medtronic and Boston Scientific and is a consultant for Abbott, outside of the submitted work. M.M.R. reports grant support and honoraria for speaking from Medtronic and Boston Scientific, outside of the submitted work. J.V. reports grants and personal fees from Medtronic Inc., grants and personal fees from Boston Scientific, personal fees from Abbott, outside of the submitted work. H.B. is consultant of Alpha-Omega, outside of the submitted work. S.C. is consultant for Medtronic and Boston Scientific, outside of the submitted work. A.H. reports lecture fees from Boston Scientific, outside of the submitted work. B.H., I.A.S., N.R., S.O., K.B., M.P., H.A., M.V., C.Z., B.S., C.F., A.A.K., M.R.D., A.M., L.M.R., L.Z., E.M.J., P.A.S., and N.L. report no competing interests.

Funding

B.H. and I.A.S. were supported via a scholarship from the Einstein Center for Neurosciences Berlin. The work conducted at the University of California San Francisco (J.L.O. and P.A.S.) received support by a grant from the Benign Essential Blepharospasm Research Foundation and philanthropic support from Larry and Kana Miao. M.V. was supported by institutional funds from Scuola Superiore Sant'Anna. Further, this work received support by the Deutsche Forschungsgemeinschaft (DFG, German Research Foundation): 424778381–TRR 295 to M.M.R., J.V, A.A.K., H.B., A.H. and NL, 347325977 to A.A.K., FI 2309/1-1 and FI 2309/2-1 to C.F. L.M.R. was supported by the Italian Ministry of Health grant GR-2009-1594645. AH was moreover supported by Deutsches Zentrum für Luft- und Raumfahrt (DynaSti grant within the EU Joint Programme Neurodegenerative Disease Research, JPND), the National Institutes of Health (R01 13478451, 1R01NS127892-01 & 2R01 MH113929) as well as the New Venture Fund (FFOR Seed Grant).

Acknowledgements

Computation has been performed on the High-Performance Compute (HCP) for Research cluster of the Berlin Institute of Health. The authors would moreover like to express their gratitude to

Charles G. Jennings, PhD, for very helpful general advice and feedback on the present work. Further, they would like to extend their thanks to the patients and their families for their participation in the clinical trials that allowed for collection of the valuable data analyzed here.

Authorship contribution statement

B.H.: Conceptualization, Writing - original draft, Data curation, Methodology, Formal analysis, Visualization, Funding acquisition. J.L.O.: Data curation, Resources, Writing - review & editing. I.A.S.: Data curation, Formal analysis, Writing - review & editing. N.R.: Methodology, Software, Resources, Data curation, Writing - review & editing. S.O.: Methodology, Software, Writing - review & editing. K.B.: Methodology, Software, Data curation, writing - review & editing. M.P., H.A., M.V., C. Z., B.S., M.M.R., & J.V.: Resources, Data curation, Writing - review & editing. C.F.: Writing - review & editing. A.A.K.: Resources, Data curation, Writing - review & editing. H.B.: Writing - review & editing. A.M., L.M.R., L.Z., E.M.J., S.C., & P.A.S.: Resources, Data curation, Writing - review & editing. N.L.: Conceptualization, Methodology, Software, Formal analysis, Resources, Data curation, Writing - original draft, Visualization, Supervision, Project administration. A.H.: Conceptualization, Methodology, Software, Resources, Data curation, Writing - original draft, Visualization, Supervision, Project administration, Funding acquisition.

References

1. Bonelli, R. M. & Cummings, J. L. Frontal-subcortical circuitry and behavior. *Dialogues Clin. Neurosci.* **9**, 141–151 (2007).
2. Haber, S. N., Liu, H., Seidlitz, J. & Bullmore, E. Prefrontal connectomics: From anatomy to human imaging. *Neuropsychopharmacology* **47**, 20–40 (2021).
3. Haynes, W. I. A. & Haber, S. N. The organization of prefrontal-subthalamic inputs in primates provides an anatomical substrate for both functional specificity and integration: Implications for basal ganglia models and deep brain stimulation. *J. Neurosci.* **33**, 4804–4814 (2013).
4. Haber, S. N. The primate basal ganglia: Parallel and integrative networks. *J. Chem. Neuroanat.* **26**, 317–330 (2003).
5. Alexander, G., DeLong, M. R. & Strick, P. L. Parallel organization of functionally segregated circuits linking basal ganglia and cortex. *Annu. Rev. Neurosci.* **9**, 357–381 (1986).
6. DeLong, M. R. Primate models of movement disorders of basal ganglia origin. *Trends Neurosci.* **13**, 281–285 (1990).
7. Parent, A. & Hazrati, L. N. Functional anatomy of the basal ganglia. I. The cortico-basal ganglia-thalamo-cortical loop. *Brain Res. Rev.* **20**, 91–127 (1995).

8. Deffains, M. *et al.* Subthalamic, not striatal, activity correlates with basal ganglia downstream activity in normal and parkinsonian monkeys. *Elife* **5**, e16443 (2016).
9. Hardman, C. D. *et al.* Comparison of the basal ganglia in rats, marmosets, macaques, baboons, and humans: Volume and neuronal number for the output, internal relay, and striatal modulating nuclei. *J. Comp. Neurol.* **445**, 238–255 (2002).
10. Deuschl, G. *et al.* A randomized trial of deep-brain stimulation for Parkinson's disease. *N. Engl. J. Med.* **355**, 896–908 (2006).
11. Ostrem, J. L. *et al.* Subthalamic nucleus deep brain stimulation in primary cervical dystonia. *Neurology* **76**, 870–878 (2011).
12. Lin, S. *et al.* Deep brain stimulation of the globus pallidus internus versus the subthalamic nucleus in isolated dystonia. *J. Neurosurg.* **132**, 721–732 (2019).
13. Mallet, L. *et al.* Subthalamic nucleus stimulation in severe obsessive-compulsive disorder. *N. Engl. J. Med.* **359**, 2121–2134 (2008).
14. Chabardes, S. *et al.* Deep brain stimulation of the subthalamic nucleus in obsessive-compulsives disorders: Long-term follow-up of an open, prospective, observational cohort. *J. Neurol. Neurosurg. Psychiatry* **91**, 1349–1356 (2020).
15. Dai, L. *et al.* Subthalamic deep brain stimulation for refractory Gilles de la Tourette' s syndrome: Clinical outcome and functional connectivity. *J. Neurol.* **269**, 6116–6126 (2022).
16. Vissani, M. *et al.* Spatio-temporal structure of single neuron subthalamic activity identifies DBS target for anesthetized Tourette Syndrome patients. *J. Neural Eng.* **16**, 066011 (2019).
17. Raichle, M. E. A brief history of human brain mapping. *Trends Neurosci.* **32**, 118–126 (2009).
18. Reid, A. T. *et al.* Advancing functional connectivity research from association to causation. *Nat. Neurosci.* **22**, 1751–1760 (2019).
19. Siddiqi, S. H., Kording, K. P., Parvizi, J. & Fox, M. D. Causal mapping of human brain function. *Nat. Rev. Neurosci.* 361–375 (2022) doi:10.1038/s41583-022-00583-8.
20. Weichwald, S. & Peters, J. Causality in cognitive neuroscience: Concepts, challenges, and distributional robustness. *J. Cogn. Neurosci.* **33**, 226–247 (2021).
21. Horn, A. & Fox, M. D. Opportunities of connectomic neuromodulation. *Neuroimage* **221**, 117180 (2020).
22. Hollunder, B. *et al.* Toward personalized medicine in connectomic deep brain stimulation. *Prog. Neurobiol.* **210**, 102211 (2022).
23. Lozano, A. M. & Lipsman, N. Probing and regulating dysfunctional circuits using deep brain stimulation. *Neuron* **77**, 406–424 (2013).
24. Horn, A. *et al.* Deep brain stimulation induced normalization of the human functional

connectome in Parkinson's disease. *Brain* **142**, 3129–3143 (2019).

25. Odekerken, V. J. J. *et al.* Subthalamic nucleus versus globus pallidus bilateral deep brain stimulation for advanced Parkinson's disease (NSTAPS study): A randomised controlled trial. *Lancet Neurol.* **12**, 37–44 (2013).
26. Kupsch, A. *et al.* Pallidal deep-brain stimulation in primary generalized or segmental dystonia. *N. Engl. J. Med.* **355**, 1978–1990 (2006).
27. Ganos, C. *et al.* A neural network for tics: Insights from causal brain lesions and deep brain stimulation. *Brain* **awac009**, (2022).
28. Goodwill, A. M. *et al.* Using non-invasive transcranial stimulation to improve motor and cognitive function in Parkinson's disease: A systematic review and meta-analysis. *Sci. Rep.* **7**, 14840 (2017).
29. Fox, M. D. *et al.* Resting-state networks link invasive and noninvasive brain stimulation across diverse psychiatric and neurological diseases. *Proc. Natl. Acad. Sci. U. S. A.* **111**, E4367–E4375 (2014).
30. Li, N. *et al.* A unified connectomic target for deep brain stimulation in obsessive-compulsive disorder. *Nat. Commun.* **11**, 3364 (2020).
31. Li, N. *et al.* A unified functional network target for deep brain stimulation in obsessive-compulsive disorder. *Biol. Psychiatry* **90**, 701–713 (2021).
32. Siddiqi, S. H. *et al.* Brain stimulation and brain lesions converge on common causal circuits in neuropsychiatric disease. *Nat. Hum. Behav.* (2021) doi:10.1038/s41562-021-01161-1.
33. Bar-Gad, I., Morris, G. & Bergman, H. Information processing, dimensionality reduction and reinforcement learning in the basal ganglia. *Prog. Neurobiol.* **71**, 439–473 (2003).
34. Horn, A. *et al.* Lead-DBS v2: Towards a comprehensive pipeline for deep brain stimulation imaging. *Neuroimage* **184**, 293–316 (2019).
35. Wang, F. *et al.* In vivo human whole-brain Connectom diffusion MRI dataset at 760 µm isotropic resolution. *Sci. Data* **8**, 122 (2021).
36. Van Essen, D. C. *et al.* The WU-Minn Human Connectome Project: An overview. *Neuroimage* **80**, 62–79 (2013).
37. Petersen, M. V *et al.* Holographic reconstruction of axonal pathways in the human brain. *Neuron* **104**, 1056-1064.e3 (2019).
38. Maier-Hein, K. H. *et al.* The challenge of mapping the human connectome based on diffusion tractography. *Nat. Commun.* **8**, (2017).
39. Middlebrooks, E. H. *et al.* Neuroimaging advances in deep brain stimulation: Review of indications, anatomy, and brain connectomics. *Am. J. Neuroradiol.* **41**, 1558–1568 (2020).
40. Neudorfer, C. *et al.* Lead-DBS v3.0: Mapping deep brain stimulation effects to local

anatomy and global networks. *Neuroimage* **268**, 119862 (2023).

41. Ewert, S. *et al.* Toward defining deep brain stimulation targets in MNI space: A subcortical atlas based on multimodal MRI, histology and structural connectivity. *Neuroimage* **170**, 271–282 (2018).
42. Amunts, K. *et al.* BigBrain: An ultrahigh-resolution 3D human brain model. *Science (80-.).* **340**, 1472–1475 (2013).
43. Horn, A. *et al.* Optimal deep brain stimulation sites and networks for cervical vs. generalized dystonia. *Proc. Natl. Acad. Sci.* **119**, e2114985119 (2022).
44. Edlow, B. L. *et al.* 7 Tesla MRI of the ex vivo human brain at 100 micron resolution. *Sci. Data* **6**, 244 (2019).
45. Baldermann, J. C. *et al.* Connectivity profile predictive of effective deep brain stimulation in obsessive-compulsive disorder. *Biol. Psychiatry* **85**, 735–743 (2019).
46. Irmen, F. *et al.* Left prefrontal connectivity links subthalamic stimulation with depressive symptoms. *Ann. Neurol.* **87**, 962–975 (2020).
47. Johnson, K. A. *et al.* Basal ganglia pathways associated with therapeutic pallidal deep brain stimulation for Tourette syndrome. *Biol. Psychiatry Cogn. Neurosci. Neuroimaging* (2020) doi:10.1016/j.bpsc.2020.11.005.
48. Baldermann, J. C. *et al.* Connectomic deep brain stimulation for obsessive-compulsive disorder. *Biol. Psychiatry* **90**, 678–688 (2021).
49. Faria, A. V. *et al.* Atlas-based analysis of resting-state functional connectivity: Evaluation for reproducibility and multi-modal anatomy-function correlation studies. *Neuroimage* **61**, 613–621 (2012).
50. Noecker, A. M. *et al.* StimVision v2: Examples and applications in subthalamic deep brain stimulation for Parkinson's disease. *Neuromodulation* **24**, 248–258 (2021).
51. Rodriguez-Oroz, M. C. *et al.* Initial clinical manifestations of Parkinson's disease: Features and pathophysiological mechanisms. *Lancet Neurol.* **8**, 1128–1139 (2009).
52. Horn, A. *et al.* Teaching NeuroImages: In vivo visualization of Edinger comb and Wilson pencils. *Neurology* **92**, e1663–e1664 (2019).
53. Zheng, T. & Wilson, C. J. Corticostriatal combinatorics: The implications of corticostriatal axonal arborizations. *J. Neurophysiol.* **87**, 1007–1017 (2002).
54. Penfield, W. & Perot, P. The brain's record of auditory and visual experience: A final summary and discussion. *Brain* **86**, 595–696 (1963).
55. Albin, R. L., Young, A. B. & Penney, J. B. The functional anatomy of basal ganglia disorders. *Trends Neurosci.* **12**, 366–375 (1989).
56. Alexander, G. E. & Crutcher, M. D. Functional architecture of basal ganglia circuits: neural sNbstrates of parallel processing. *Trends Neurosci.* **13**, 266–271 (1990).
57. Percheron, G. & Filion, M. Parallel processing in the basal ganglia: Up to a point. *Trends*

Neurosci. **14**, 55–56 (1991).

58. Joel, D. & Weiner, I. The organization of the basal ganglia-thalamocortical circuits: Open interconnected rather than closed segregated. *Neuroscience* **63**, 363–379 (1994).
59. van Wijk, B. C. M., Alkemade, A. & Forstmann, B. U. Functional segregation and integration within the human subthalamic nucleus from a micro- and meso-level perspective. *Cortex* **131**, 103–113 (2020).
60. Hassler, R., Riechert, T., Mundinger, F., Umbach, W. & Ganglberger, J. A. Physiological observations in stereotaxic operations in extrapyramidal motor dysturbances. *Brain* **83**, 337–350 (1960).
61. Horn, A. *et al.* Connectivity predicts deep brain stimulation outcome in Parkinson's disease. *Ann. Neurol.* **82**, 67–78 (2017).
62. Treu, S. *et al.* Deep brain stimulation: Imaging on a group level. *Neuroimage* **219**, 117018 (2020).
63. Vanegas-Arroyave, N. *et al.* Tractography patterns of subthalamic nucleus deep brain stimulation. *Brain* **139**, 1200–1210 (2016).
64. Shirota, Y. *et al.* Supplementary motor area stimulation for Parkinson disease: A randomized controlled study. *Neurology* **80**, 1400–1405 (2013).
65. Nachev, P., Kennard, C. & Husain, M. Functional role of the supplementary and pre-supplementary motor areas. *Nat. Rev. Neurosci.* **9**, 856–869 (2008).
66. Corp, D. T. *et al.* Network localization of cervical dystonia based on causal brain lesions. *Brain* **142**, 1660–1674 (2019).
67. Okromelidze, L. *et al.* Functional and structural connectivity patterns associated with clinical outcomes in deep brain stimulation of the globus pallidus internus for generalized dystonia. *Am. J. Neuroradiol.* **41**, 508–514 (2020).
68. Inoue, K. *et al.* Disinhibition of the somatosensory cortex in cervical dystonia - decreased amplitudes of high-frequency oscillations. *Clin. Neurophysiol.* **115**, 1624–1630 (2004).
69. Prudente, C. N., Hess, E. J. & Jinnah, H. A. Dystonia as a network disorder: What is the role of the cerebellum? *Neuroscience* **260**, 23–35 (2014).
70. Neychev, V. K., Fan, X., Mitev, V. I., Hess, E. J. & Jinnah, H. A. The basal ganglia and cerebellum interact in the expression of dystonic movement. *Brain* **131**, 2499–2509 (2008).
71. Havrankova, P. *et al.* Repetitive TMS of the somatosensory cortex improves writer's cramp and enhances cortical activity. *Neuroendocrinol. Lett.* **31**, 73–86 (2010).
72. Bradnam, L. V., McDonnell, M. N. & Ridding, M. C. Cerebellar intermittent theta-burst stimulation and motor control training in individuals with cervical dystonia. *Brain Sci.* **6**, 56 (2016).
73. Desrochers, P., Brunfeldt, A., Sidiropoulos, C. & Kagerer, F. Sensorimotor control in

dystonia. *Brain Sci.* **9**, 79 (2019).

74. Carmi, L. *et al.* Efficacy and safety of deep transcranial magnetic stimulation for obsessive-compulsive disorder: A prospective multicenter randomized double-blind placebo-controlled trial. *Am. J. Psychiatry* **176**, 931–938 (2019).
75. McGovern, R. A. & Sheth, S. A. Role of the dorsal anterior cingulate cortex in obsessive-compulsive disorder: Converging evidence from cognitive neuroscience and psychiatric neurosurgery. *J. Neurosurg.* **126**, 132–147 (2017).
76. Franzkowiak, S. *et al.* Motor-cortical interaction in Gilles de la Tourette syndrome. *PLoS One* **7**, e27850 (2012).
77. Worbe, Y. *et al.* Altered structural connectivity of cortico-striato-pallido-thalamic networks in Gilles de la Tourette syndrome. *Brain* **138**, 472–482 (2015).
78. Andrade, P. *et al.* Modulation of fibers to motor cortex during thalamic DBS in Tourette patients correlates with tic reduction. *Brain Sci.* **10**, 302 (2020).
79. Jo, H. J. *et al.* Global network modulation during thalamic stimulation for Tourette syndrome. *NeuroImage Clin.* **18**, 502–509 (2018).
80. Johnson, K. A. *et al.* Structural connectivity predicts clinical outcomes of deep brain stimulation for Tourette syndrome. *Brain* **143**, 2607–2623 (2020).
81. Kleimaker, M. *et al.* Non-invasive brain stimulation for the treatment of Gilles de la Tourette syndrome. *Front. Neurol.* **11**, 592258 (2020).
82. Martino, D., Ganos, C. & Worbe, Y. Neuroimaging applications in Tourette's syndrome. *Int. Rev. Neurobiol.* **143**, 65–108 (2018).
83. Cavanna, A. E., Black, K. J., Hallett, M. & Voon, V. Neurobiology of the premonitory urge in Tourette's syndrome: Pathophysiology and treatment implications. *J. Neuropsychiatry Clin. Neurosci.* **29**, 95–104 (2017).
84. Percheron, G., Yelnik, J. & François, C. A Golgi analysis of the primate globus pallidus. III. Spatial organization of the striato-pallidal complex. *J. Comp. Neurol.* **227**, 214–227 (1984).
85. Ashkan, K., Rogers, P., Bergman, H. & Ughratdar, I. Insights into the mechanisms of deep brain stimulation. *Nat. Rev. Neurol.* **13**, 548–554 (2017).
86. Neudorfer, C. *et al.* Kilohertz-frequency stimulation of the nervous system: A review of underlying mechanisms. *Brain Stimul.* **14**, 513–530 (2021).
87. Husch, A., V. Petersen, M., Gemmar, P., Goncalves, J. & Hertel, F. PaCER - A fully automated method for electrode trajectory and contact reconstruction in deep brain stimulation. *NeuroImage Clin.* **17**, 80–89 (2018).
88. Ewert, S. *et al.* Optimization and comparative evaluation of nonlinear deformation algorithms for atlas-based segmentation of DBS target nuclei. *Neuroimage* **184**, 586–598 (2019).

89. Vogel, D. *et al.* Anatomical brain structures normalization for deep brain stimulation in movement disorders. *NeuroImage Clin.* **27**, 102271 (2020).
90. Tyagi, H. *et al.* A randomized trial directly comparing ventral capsule and anteromedial subthalamic nucleus stimulation in obsessive-compulsive disorder: Clinical and imaging evidence for dissociable effects. *Biol. Psychiatry* **85**, 726–734 (2019).
91. Avants, B. B., Epstein, C. L., Grossman, M. & Gee, J. C. Symmetric diffeomorphic image registration with cross- correlation: Evaluating automated labeling of elderly and neurodegenerative brain. *Med. Image Anal.* **12**, 26–41 (2008).
92. Fonov, V. *et al.* Unbiased average age-appropriate atlases for pediatric studies. *Neuroimage* **54**, 313–327 (2011).
93. Horn, A. & Kühn, A. A. Lead-DBS: A toolbox for deep brain stimulation electrode localizations and visualizations. *Neuroimage* **107**, 127–135 (2015).
94. Vorwerk, J., Oostenveld, R., Piastra, M. C., Magyari, L. & Wolters, C. H. The FieldTrip-SimBio pipeline for EEG forward solutions. *Biomed. Eng. Online* **17**, 37 (2018).
95. Yeh, F.-C. *et al.* Quantifying differences and similarities in whole-brain white matter architecture using local connectome fingerprints. *PLoS Comput. Biol.* **12**, e1005203 (2016).